


 Cite this: *Sens. Diagn.*, 2023, 2, 268

## Diagnosis of cancer using carbon nanomaterial-based biosensors

 Suman Das, <sup>†ab</sup> Bijay Saha, <sup>†c</sup> Manisha Tiwari<sup>a</sup> and Dharmendra K. Tiwari <sup>\*a</sup>

Cancer causes the death of a large population worldwide. Early-stage tumor detection is the major problem in treating cancer patients effectively. Nanomaterial-based biosensors have emerged as a great tool for diagnosis of many life-threatening diseases including cancer. Various carbon nanomaterial-based biosensors have been evolved for cancer detection; these increase the accuracy of diagnosis in the very early stage of tumor detection. The most common carbon nanomaterial-based biosensors are electrochemical and optical sensors. These biosensors are portable and biocompatible with a long shelf-life and show efficient results in cancer detection, diagnosis, management and treatment. In this review, we summarize various types of electrochemical and optical carbon nanomaterial sensors and their applications, efficiency and usability. This review will also give the background of their fabrication, synthesis and shelf-life, which will help researchers and medical experts to improve and utilize them for cancer diagnosis.

 Received 21st October 2022,  
 Accepted 12th December 2022

DOI: 10.1039/d2sd00182a

[rsc.li/sensors](https://rsc.li/sensors)

### 1. Introduction

In the last few years, cancer has emerged as the most life-threatening disease all over the world. There are more than

200 types of cancers listed to date including breast, ovarian, skin, hematologic, prostate, lung, leukemia, and colon cancers, affecting different body parts and thousands of deaths are occurring each day. Osteosarcoma, the most common primary bone cancer, occurs in different body parts like the proximal humerus, around the knee and the proximal tibia, and is largely observed in children, but can also affect older adults.<sup>1,2</sup> There are many factors which may be taken into account for the cause of cancer such as autoimmune dysfunction, inherited mutations and some environmental factors like exposure to carcinogenic chemicals or certain radiation. Manifestations of various viral

<sup>a</sup> Department of Biotechnology, School of Biological Science and Biotechnology, Goa University, Taleigao Plateau, Goa 403206, India. E-mail: dktiwari@unigoa.ac.in, dharmendratiwari@gmail.com

<sup>b</sup> Department of Cell Biology, Helmholtz Centre for Infection Research, Braunschweig, 38124 Germany

<sup>c</sup> Department of Chemistry, Central University of Punjab, VPO-Ghudda, Bathinda 151401, India

† These authors contributed equally to this work.


**Suman Das**

Suman Das received his Master's degree in Life Sciences (specialization in Molecular Medicine) from the Central University of Punjab, India, in 2019. Currently, he is working as a Doctoral Researcher at the Department of Cell Biology, Helmholtz Centre for Infection Research, Braunschweig, Germany. Before moving to Germany, he was working as a Project Assistant at the Department of Biotechnology,

Goa University, India. His research interests are mainly focused on cell biology, cellular immunology, actin cytoskeleton, cancer biology, photodynamic therapy, and BRET photosensitizer development.


**Bijay Saha**

Bijay Saha received his Master's degree in Applied Chemistry from the Central University of Punjab, Punjab in 2020. He received his Bachelor's degree in Chemistry from Bangabasi College, Calcutta University, West Bengal in 2018. He worked on a project titled "Photocatalytic degradation of toxic dyes using biopolymer-based nanocomposite". His current research interests are bionanotechnology and synthesis of nanomaterials for biomedical

applications.



and bacterial infections are also responsible for the cause of stomach and cervical cancers. Disruption of normal cell signaling pathways leads to the production of cancer cells that exhibit higher growth advantages as compared to the normal cells. Cancer cells are produced from some different epigenetic and/or genetic changes which cause inactivation of tumor suppressor genes and activation of oncogenes. However, in the case of diagnosis, various genes are universally altered during this process, and the pattern of change is not the same for tumors in different organs as well as for tumors in the same location.<sup>3</sup> According to the WHO, over 9.6 million deaths were registered in 2018 and most of the cancer deaths are lung (1.76 million deaths), colorectal (862 000 deaths), liver (782 000 deaths), breast (627 000 deaths), and stomach (783 000 deaths) cancers. Therefore, early detection of cancer is of utmost importance to monitor the health condition of a patient as well as for a successful treatment. Due to these reasons, more specific and sensitive techniques are needed for the detection of this disease at a very early stage. In the field of medical science, diagnosis of a disease can be performed by detecting responsible biomarkers present in urine, cerebrospinal fluid (CSF), blood and other body fluids, which is considered as a very easy and effective method. CD44 is considered as a promising surface biomarker for the diagnosis of breast cancer stem cells (BCSCs).<sup>4</sup> Apolipoprotein-A1 (Apo-A1) is a new biomarker which is very prominent for the early diagnosis of bladder cancer from human urine.<sup>5</sup> CA15-3 is considered the most effective biomarker for breast cancer detection at a concentration level of  $>100 \text{ U mL}^{-1}$ .<sup>6,7</sup> For the diagnosis of cancer, existing methods rely on traditional procedures *i.e.* cell morphology with the help of staining and microscopy. These are the techniques based on biopsy and examination of the tissue morphology, which can miss the cancer cells in their earlier stages. There are some recent techniques using

immunoassays that are very sensitive and selective towards the low concentration of cancer biomarkers but can be expensive and time-consuming. Western blotting, immunohistochemistry (IHC), radioimmunoassay (RIA), enzyme-linked immunosorbent assay (ELISA), high-performance liquid chromatography (HPLC), and polymerase chain reaction (PCR) are the conventional techniques used for the identification of biomarkers with certain technical limitations. To overcome these challenges a rapid and sensitive as well as point of care technology is required for rapid diagnosis. In the last few years, Scopus showed that more than 2500 research articles have been published on biosensors, which have been developed in the fields of clinical diagnosis and biomedical studies due to their high selectivity, sensitivity, faster response, easy handling, and compatibility. Naderi and Jalali developed a modified glassy carbon electrode (GCE) using poly L-serine, AuNPs and multi-walled carbon nanotubes (MWCNTs) for electrochemical detection of progesterone which is commonly used for the confirmation of pregnancy.<sup>8,9</sup> From point of care (POC) diagnosis, biosensors would be a very cost-effective and rapid tool for the detection of a disease. A biosensor is an analytical device, where a bio-receptor is incorporated and integrated with a transducer. The affinity between complementary structures like antigen-antibody, enzyme-substrate, and receptor-hormone is controlled by the specific molecular recognition, which is the fundamental part of biosensing and also responsible for the generation of concentration-proportional signals in biosensors. The specificity and selectivity of biosensors towards the detection of biomarkers extremely depend on this molecular recognition part connected to the transducer.<sup>10</sup>

Different types of nanomaterials are used in biosensors for clinical diagnosis such as gold, iron,<sup>11</sup> silicon,<sup>12</sup> magnetic materials, quantum dots,<sup>11</sup> 2D nanomaterials, nickel



**Manisha Tiwari**

*Manisha Tiwari received her Master's degree in Microbiology from Kanpur University (India), in 2006. She worked at Osaka University as a visiting research fellow from 2008–2009. She received her PhD degree from Hokkaido University, Japan in 2013. She moved to Osaka and worked as a postdoctoral fellow at Quantitative Biology Centre, RIKEN, Osaka. Currently, she is working as a Woman Scientist (DBT-BioCARE) at the*

*Department of Biotechnology, Goa University, India. Her research interests are luminescence and fluorescence-based biosensors, cell-receptor dynamics, fluorescence imaging, optical microscopy imaging and FCCS to explore molecular and cellular mechanisms.*



**Dhermendra K Tiwari**

*Dhermendra K Tiwari received his Ph.D. degree from Jawaharlal Nehru University, New Delhi. He was a postdoctoral fellow at Hokkaido University (Japan), Osaka University (Japan) and NUS (Singapore). At present he is a UGC-Assistant Professor and Ramalingaswami Re-entry Fellow funded by Govt. of India, at the Department of Biotechnology, Goa University, India. His research interests are nanobiotechnology, fluorescence*

*and luminescence probe development for cellular application, photodynamic therapy-based probe development, antimicrobial-PDT, and photosensitive molecules and nanomaterials for biomedical applications and mechanobiology studies.*



hexacyanoferrate nanoparticles (NiHCFNPs),<sup>13</sup> *etc.* due to their higher efficiency, higher detection limit of an analyte, higher stability and lower cost. Several carbon-based nanomaterials have been explored several times due to their exclusive properties and used as a major component in biosensors for clinical diagnosis of diseases such as cancer (Table 1) with over 100 published research articles.

Due to the presence of unique chemical, optical and physical properties, a large range of carbon-based materials such as nanodiamonds, carbon nanotubes (SWNTs and MWNTs), fullerenes, carbon onions,<sup>14</sup> quantum dots like carbon dots (CDs), and graphene quantum dots (GQDs)<sup>15</sup> have been explored for the detection of cancer. Considering these properties of carbon-based nanomaterials, here we aim to discuss the recent advancements of carbon-based nanomaterials in the diagnostic field of cancer.

## 2. Carbon-based nanomaterials

Nanoparticles are small particles having a size range between 1 and 100 nm.<sup>16</sup> The advancement of nanomaterials towards biomedical applications has created a new era in the field of medical science due to their extraordinary characteristics. The higher surface to volume ratio, easy derivatization, and higher thermal and mechanical stability makes nanomaterials unique from other substances. Carbon is an essential element in nature and has been targeted by humans to develop its use in the medical field as well as environmental research with the help of advanced technology for a long time. With the development of nanoscience, the size of carbon materials has changed from the microscopic level to the nano level. Carbon-based nanomaterials, one of the significant parts of nanotechnology, have attracted the scientific world since their discovery. Nowadays, various allotropes of carbon with specific dimensions (0D, 1D, 2D, 3D) and different hybridization such as  $sp$ ,  $sp^2$ , and  $sp^3$  have been reported. In recent years, a large number of carbon allotropes have been explored including very well-known allotropic phases graphite, fullerene, and diamond to newly discovered nanodiamonds, carbon nanobuds, graphene, graphene oxide, carbon nanocones, carbon nanotubes (CNTs), and quantum dots as well as their functionalized forms<sup>17</sup> and have been applied in many different fields such as field emission display, nano-electronics and high-frequency electronics,<sup>18,19</sup> theragnostics,<sup>20</sup> and energy storage and conversion.<sup>21</sup> In the last few decades, carbon-based materials have played a significant role in biosensor research for enhancing reactivity and specificity. On the basis of their salient properties, the uses of these materials in biosensors have regularly expanded from building blocks to electrode materials (Fig. 1).

### 2.1. Graphene

About 70 years ago, in 1947 the electronic structure of graphene was evaluated by Wallace and McClure, who later assumed the expression of the wave equation in 1956.

Mouras and co-workers first introduced the name “graphene” in 1987 in the form of “graphitic intercalation compounds (GICs)”.<sup>22</sup> Graphene is a single layer of carbon atoms that are closely packed in a honeycomb type of lattice in two dimensions or in other words a single layer of graphite sheet having an  $sp^2$  hybridized carbon arrangement with an interlayer distance of 3.4 Å and a carbon–carbon bond distance of 1.42 Å.<sup>23</sup> The first graphene was synthesized by Geim and coworkers using mechanical exfoliation of well-oriented pyrolytic graphite which is also known as the scotch-tape method.<sup>24</sup> Graphene nanomaterials have been selectively used for electrochemical sensing of RNA and DNA which is based on the strong ionic interaction between positively charged nucleobases and negatively charged carboxylic groups as well as strong  $\pi$ – $\pi$  interaction between the carbon framework and nucleobases.<sup>25,26</sup> Graphene-based electrodes have been used for the detection of biomolecules including  $H_2O_2$ , NADH, and dopamine due to the higher electrochemical selectivity and sensitivity of graphene.<sup>27</sup> The use of graphene oxide (GO)-based nanomaterials for the detection of glucose levels in the human body is now increasing prosperously.<sup>28</sup> For field-effect transistors, graphene is the ideal material due to its zero bandgap and it can be tuned by surface modification.<sup>29</sup> Label-free DNA biosensors have been designed by Johnson and co-workers based on single-stranded probe DNA functionalized graphene field-effect transistors. This extremely sensitive sensor represents a wide analytical range of detection limit of 1 femtomolar (fM) for 60 mer DNA oligonucleotides.<sup>30</sup>

### 2.2. Carbon nanotubes (CNTs)

Carbon nanotubes (CNTs) have attracted the attention of scientists in numerous applications in different research areas due to their exceptional properties including thermal, mechanical and chemical properties since their discovery. Iijima and coworkers first discovered carbon nanotubes, which are also called bucky tubes, in 1991.<sup>31</sup> From a theoretical explanation, carbon nanotubes are hollow tube structures made up of graphene sheets, with one or more walls. They show a strong-layered structure due to the presence of linked  $sp^2$  hybridized carbon–carbon bonds, which makes CNTs strongest and stiffest. Nowadays, multi-walled-CNTs (MWCNTs) and single-walled-CNTs (SWCNTs) are manufactured by high-temperature processes such as laser ablation, electric arc discharge and chemical vapor deposition (CVD).<sup>32</sup> There are two types of CNTs depending on layers; one is MWCNTs which consist of a group of concentric cylinders with a usual periodic interlayer space, sharing a common axis (Fig. 2C).<sup>33</sup> From real space analysis, the interlayer spacing of MWNCNTs was observed in the range of 0.34 nm to 0.39 nm.<sup>34</sup> Considering the number of layers, the inner and outer diameters of MWCNTs change from 0.4 nm to a few nanometers, and 2 nm to 30 nm, respectively.<sup>35</sup> On the other hand, SWCNTs are characterised as a well-organized, hollow graphite material, by folding up a



**Table 1** Showing different carbon-based materials used for the detection of various cancer biomarkers

Biomarker	Carbon material	Detection technique	Detection level	Reference
TP53	Reduced graphene oxide-carboxymethylcellulose (rGO-CMC) hybrid nanomaterial	Amperometry	2.9 nM-3.4 nM	117
mir-21	Graphene-modified pencil graphite electrode (GME)	Differential pulse voltammetry (DPV) and electrochemical impedance spectroscopy (EIS)	2.09 mg mL <sup>-1</sup>	118
VEGFR2	Chitosan functionalized reduced graphene oxide	Voltammetric technique	0.28 pM	119
Prostate-specific antigen (PSA)	Magnetic graphene oxide-PSMA <sub>ab</sub>	Differential pulse voltammetry (DPV)	10 pg mL <sup>-1</sup>	120
CYFRA-21-1	3-Aminopropyl triethoxy saline (APTES) functionalized rGO-zirconia (ZrO <sub>2</sub> ) based nanocomposite	Differential pulse voltammetry (DPV)	2-22 ng mL <sup>-1</sup>	121
CEA	AuNP functionalized magnetic MWCNTs containing Pb(II) modified glassy carbon electrode(Pb <sup>2+</sup> @Au@MWCNTs-Fe <sub>3</sub> O <sub>4</sub> )	Cyclic voltammetry and amperometric curve	1.7 fg mL <sup>-1</sup>	128
CEA	GO/MWCNT-COOH/Au@CeO <sub>2</sub> nanocomposite	Electrochemiluminescence	0.02 ng mL <sup>-1</sup>	129
CEA	Ag NPs-MWCNTs/MnO <sub>2</sub>	Amperometric curve	0.03 pg mL <sup>-1</sup>	130
Prostate-specific antigen (PSA)	rGO-MWCNT/AuNPs	Electron transfer resistance (R <sub>ct</sub> ) and differential pulse voltammetry (DPV)	1 pg mL <sup>-1</sup>	131
Alpha-fetoprotein (AFP)	PLL-SWCNTs	Differential pulse voltammetry (DPV) and electrochemical impedance spectroscopy (EIS)	0.011 ng mL <sup>-1</sup>	132
miRNA-24	MWCNT-modified glass carbon electrodes	Differential pulse voltammetry (DPV)	1 pM mL <sup>-1</sup>	133
PSA	Au/Ag-rGO/aminated-GQDs/carboxyl-GQDs	Electrochemiluminescence	0.29 pg mL <sup>-1</sup>	132
CEA	GQDs/Au@Pt	Electrochemiluminescence	0.6 pg mL <sup>-1</sup>	133
CA199	GQD functionalized pPtPd nanochains	Electrochemiluminescence	0.96 mU mL <sup>-1</sup>	140
miRNA-155	GQDs	Amperometry	0.14 fM	141
IL-13R $\alpha$ 2	GQD functionalized MWCNTs	Amperometry	0.8 ng mL <sup>-1</sup>	142
miRNA-141	GO-AuNPs	Surface plasmon resonance (SPR)	1 fM	145
Cytokeratin 19 (CK19)	Carboxyl-functionalized graphene oxide (GO-COOH)	Surface plasmon resonance (SPR)	1 fg mL <sup>-1</sup>	147
Folic acid protein (FAP)	(Au/rGO)	Surface plasmon resonance (SPR)	5 fM	148
Pyrophosphate (PPi)	PDI-HIS-Cu-GO nanocomposites	Fluorescence spectroscopy	0.60 $\times$ 10 <sup>-7</sup> M	150
Urokinase plasminogen activator (uPA)	ssDNA-SWCNT	Fluorescence spectroscopy	50 nM	151
CA125	Three-dimensional network of carbon nanotubes (3DNCNTs)	Fluorescence spectroscopy	20 $\mu$ g mL <sup>-1</sup>	152
mir19 and R23 RNA	SWCNTs	Photoluminescence	0.02 mg mL <sup>-1</sup>	153
Leukemia K562 cells	3-Glycidoxypropyl trimethoxysilane (GPMS) functionalized CNTs	Photoconductivity	27cells per ml	154
PSMA	Functionalized MWCNTs	Electrochemiluminescence	0.88 ng mL <sup>-1</sup>	156
CEACAM5	VA-MWCNT	Cyclic voltammetry (CV) and electrochemical impedance spectra (EIS)	0.92 $\mu$ M	136
MALAT1	Au NCs/MWCNT-NH <sub>2</sub>	Cyclic voltammetry (CV)	42.8 fM	137
Transmembrane protein CD63	SWNTs	UV-vis spectrometry	5.2 $\times$ 10 <sup>5</sup> particles per $\mu$ L	157
MMP-7, MMP-2, uPA	Peptide-MWCNT nanoprobes	Fluorescence spectroscopy	0.5 pg mL <sup>-1</sup>	158
$\beta$ -Glucuronidase (GLU)	Nitrogen-doped carbon quantum dots (N-CQDs)	Photoluminescence	0.3 U L <sup>-1</sup>	161
Carbohydrate antigen 15-3 (CA15-3)	Graphene oxide-PEI-carbon quantum dot (CQD)-Au nanohybrid	Electrochemiluminescence	0.0017 U mL <sup>-1</sup>	162
K562 leukemia cells	ZnO@CQDs	Electrochemiluminescence	46 cells per mL	163
miRNA-155	C-dot-MnO <sub>2</sub> nanosheets	FRET	0.1 $\times$ 10 <sup>-18</sup> M	164
Mucin 1 protein	Aptamer-CDs	FRET	17.1 nM	165
$\alpha$ -L-Fucosidase (AFU)	AuNP functionalized CDs	Fluorescence emission spectroscopy	3.4 nM	166
BRCA1 and BRCA2	Graphene-coated optical fiber	Surface plasmon resonance (SPR)	1-100 nM	146



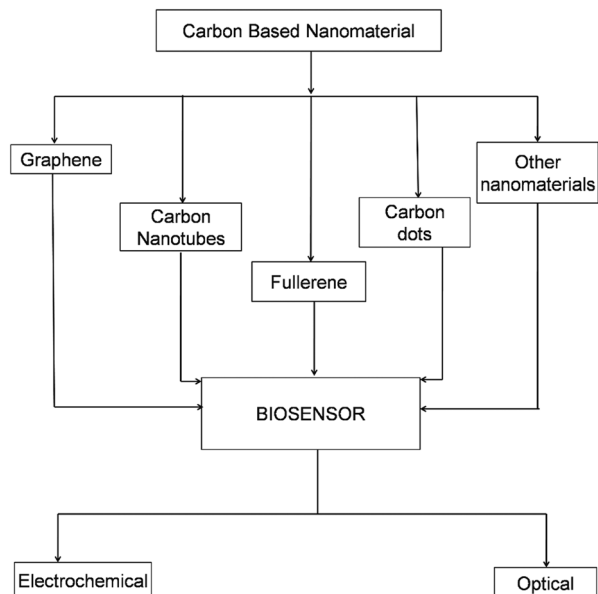


Fig. 1 Flowchart showing the classification of biosensors developed from carbon-based nanomaterials.

graphene sheet along a lattice vector into a cylindrical form having diameters ranging from 0.4 to 3 nm and lengths falling in the micrometer range of up to 20 cm.<sup>36</sup> SWCNTs can form a bundle (rope)-like structure where they are hexagonally organized which helps bundle-like structures to form a crystal-like configuration.<sup>37</sup> A single wall can exist in three different forms depending on the way of wrapping to a cylinder such as chiral, zigzag, and armchair. A SWCNT is described by a pair of indices ( $n$  &  $m$ ) that depict the chiral vector and control the electronic properties. If  $m = 0$ , then the nanotubes are zigzag nanotubes; when  $m = n$ , then the nanotubes are named as an armchair, and the rest of the configurations are chiral when  $m \neq n$  (Fig. 2A).<sup>33</sup> There is another special class of nanotubes called doubled-walled carbon nanotubes (DWNTs), made up of two concentric cylinders (Fig. 2B).<sup>33</sup> DWNTs connect SWCNTs and MWCNTs and show properties of both kinds of CNTs. The diameter of DWNTs is quite similar to that of SWCNTs but they largely differ in mechanical stability.<sup>38</sup> Besides this, the immobilization of large functional molecules such as receptor moieties at the surface of CNTs is highly favorable due to their higher surface area, which is an important part of biosensing application. CNTs have electrical conductivity that makes them perfect for the transduction of electrical signals formed after recognition of the target analyte. A various number of functionalized CNT-based biosensors such as electrochemical CNT-biosensors, immunosensors, FET biosensors and optical biosensors have been developed for the detection of different enzymes, proteins, DNA biomarkers and cell-surface sugars.<sup>33</sup> Feng and coworkers introduced a disposable paper-based bipolar electrode (BPE) modified with MWNTs for the detection of prostate-specific antigen (PSA) that showed a significant response in the sensitive electro-

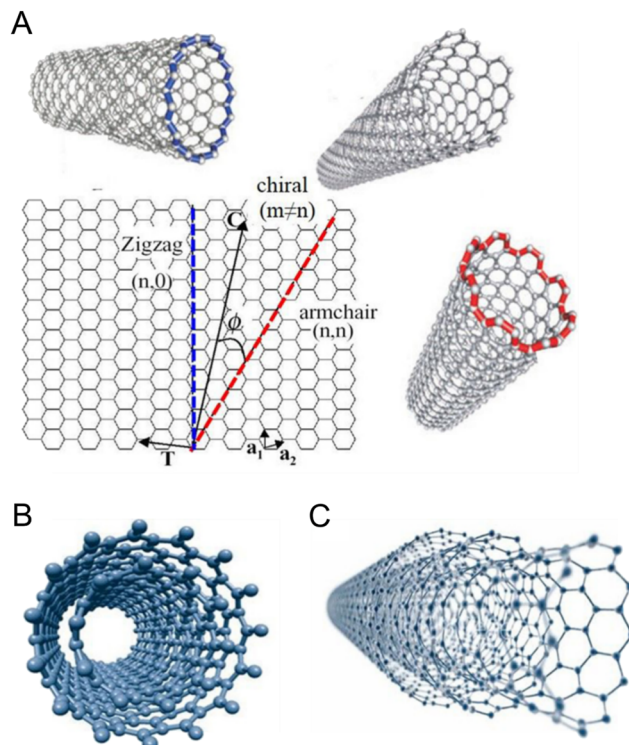


Fig. 2 Different structures of carbon nanotubes in terms of their number of walls. (A) Single-walled carbon nanotube (SWCNT) structures according to their chirality (chiral, zigzag and armchair). (B) Model of double-walled carbon nanotubes (DWNTs). (C) Structure of multi-walled carbon nanotubes (MWNTs) consisting of many concentric shells. Reproduced from ref. 33 with permission from Frontiers Media S.A., copyright [2015].<sup>33</sup>

chemiluminescence (ECL) detection having a detection limit of  $1 \text{ pg mL}^{-1}$ .<sup>39</sup> Recently, Shobha and coworkers reported the properties of both MWNTs and SWNTs for the earlier detection of prostate cancer, through functionalization with DNA strands that detect the PSA concentration level present in blood samples.<sup>40</sup> Unfunctionalized SWNTs exhibit low intensity, fluorescence stability, and biocompatibility whereas surface functionalization or modification changes the interactions with the target analyte and affects the SWNT fluorescence emission signals significantly,<sup>41,42</sup> and therefore functionalized CNT materials are best candidates for fluorescence-based sensing applications.<sup>43,44</sup>

### 2.3. Fullerene

Several numbers of 0D, 1D, and 2D carbon materials have been developed such as carbon nanotubes, graphene, nanowires, and nanoclusters for the betterment of the application field. Fullerenes are also very potent active members of this carbon nanostructure family. Fullerenes are extremely symmetrical polyhedral clusters or closed cage-like structures where each  $\text{sp}^2$  hybridized carbon atom bonded in an arrangement of fused six and five-membered rings and these rings are formed by a total of 70 and 60 atoms, known as C70 and C60, respectively.<sup>45</sup> The next stable homolog after



C60 is C70 followed by C74, C76, C80, C82, and so on.<sup>46</sup> Since their invention, fullerenes having extraordinary electrochemical properties and stability have attracted so many researchers. Geodesic and electronic bonding is responsible for the stability of C60 molecules. In 1966, Daedalus proposed a scheme for making a large hollow carbon cage. Later on, Osawa first introduced the  $I_h$  symmetric soccer-like structure of the C60 molecule in 1970. In 1985, the final breakthrough occurred in the discovery of fullerene C60 by Kroto and Smalley during the process of vaporizing graphite using an Nd:YAG laser. It was also named as buckminsterfullerene because architect R. Buckminster Fuller designed its structure<sup>47</sup> which is very similar to a soccer ball. The  $sp^2$ -hybridized carbon formed an extended  $\pi$ - $\pi$  conjugation, which makes it a good electron acceptor. Nowadays, fullerenes are being used in numerous research fields including solar cells, biomedical applications, nanoelectronics and supercapacitors. Fullerenes show high potential biological activity due to their low diameter (7–10 Å) and higher opportunities in surface chemical modification.<sup>48</sup>

In C60, two different bond lengths are observed, one is 6:6 ring bonds which can be treated as double bonds that are shorter as compared to 6:5 bonds. C60 is not considered as a super aromatic molecule because it tends to avoid double bonds in pentagonal rings, ensuring poor electron delocalization. Hence, C60 structures always behave as an electron-deficient alkene and easily react with electron-rich species. The experimental values of ionization potential (IP) 7.8 eV and electron affinity (EA) 2.7 eV of C60 revealed that they can easily take part in electron transfer reactions and also showed high electrochemistry which makes them active members for electrochemical applications.<sup>49–51</sup>

The most broadly used procedure for the preparation of fullerenes is primarily based on the arc plasma vaporization of high carbon content materials like coal or graphite at low inert gas pressure, but in this method the yield of pure fullerenes is quite low. For better results and large scale synthesis of fullerenes, high-frequency arc plasma-based processes are used.<sup>52</sup> There are other synthesis procedures that have been introduced based on chemical synthesis, reactive precursors, and vaporization of carbon sources.<sup>53,54</sup>

Since the discovery of fullerenes (C60), a drastic change has been observed in the research field of biosensors. The exceptional topological attributes and electrochemical characteristics of fullerenes such as photo-thermal effect, broad light absorption in the UV-vis region, a higher lifetime of the triplet state, structural angular strain, and tendency to act as electrophilic as well as nucleophilic characteristics have attracted large interest of researchers to investigate this material as a mediator in biosensor devices.<sup>55</sup> To make fullerene as an effective mediator in a biosensing device, hydrophilicity and the presence of functional groups were considered as important qualities in order to combine them with the targeted biomolecules. But these two characteristics are absent resulting in inefficient bioconjugation with biologically active molecules.<sup>56</sup> To overcome this difficulty,

functionalization is highly needed with carboxy, amino or hydroxyl groups. The methodology of functionalization may vary depending on the area of application. Depending upon the analyte (enzyme, protein, antigen, *etc.*) and type of biosensor (potentiometric, electrochemical, optical), the elemental fullerene is modified with necessary functional groups so that they can suitably approach the target molecule. As a result, there will be a sufficient electron transfer between electrodes and the analyte.<sup>57</sup> In the case of a glucose biosensor, the fullerene is immobilized against the glucose oxidase enzyme. It is reported that the sensitivity of the glucose biosensor increases with the increase in immobilization concentration of fullerenes.<sup>58</sup> Fullerenes have also been tested for urea detection using potentiometric as well as piezoelectric biosensors. In a potentiometric biosensor, a fullerene-urease bioconjugate was used on an acrylic-based hydrogen ion membrane for the detection of urea and the results showed that this conjugate is stable up to 140 days.<sup>59</sup> Besides electrochemical, potentiometric or piezoelectric biosensors, there are many biosensors including immunosensors<sup>57</sup> and DNA sensors,<sup>60</sup> where fullerenes play a key role in the detection of biomolecules. The signal modification, light-induced switching, and easy functionalization capabilities of fullerenes are acknowledged as a new and striking element in the modification or fabrication of biosensors.

#### 2.4. Carbon dots

The new member of the fluorescent carbon family is carbon dots denoted as C-dots having a diameter of below 10 nm.<sup>61</sup> Carbon dots are a better alternative and become the most promising material as compared to other toxic metal-based quantum dots due to their biocompatibility and composition.<sup>62</sup> The structural analysis of carbon dots makes it clear that a structural disorder occurs in the conjugation of aromatic regions with graphene-like  $sp^2$  hybridized bonds and aliphatic regions with diamond-type- $sp^3$  hybridized bonds.<sup>63</sup>

Carbon dots were derived accidentally during the synthesis of carbon nanotubes by the arc discharge method.<sup>64</sup> Basically, the effective pathways for the synthesis of carbon dots are usually divided into two main parts: one is a top-down method from the larger carbon structure (Fig. 3A)<sup>65</sup> and another is a bottom-up method where the organic molecular precursor is used as a starting material.<sup>61</sup> Top-down methods consist of three main techniques: (i) the arc-discharge method, where raw materials are oxidized with  $HNO_3$  to introduce carboxyl functional groups which enhance the hydrophilicity of the material, (ii) the laser ablation method, where a 1064 nm wavelength and 10 Hz Q-switched Nd:YAG laser is applied to ablate the carbon material in the presence of water vapor at a temperature of 900 °C and 75 kPa pressure in a flow of argon gas, followed by  $HNO_3$  activation, and the subsequent passivation is also done with the help of polymeric agents such as diamine-terminated poly(ethylene glycol),<sup>62</sup> and (iii) electrochemical synthesis, where an intense electric field helps





Fig. 3 Synthesis of graphene nanodots/carbon nanodots. (A) Top-down method and (B) bottom-up method. Reproduced from ref. 65 with permission from The Royal Society of Chemistry, copyright [2012].<sup>65</sup>

to cut the precursor material for the synthesis of carbon dots.<sup>66</sup> Bottom-up approaches are more diverse in nature (Fig. 3B).<sup>65</sup> These approaches are: (i) the microwave-assisted method from the carbon source with glycerol, (ii) ultrasonic synthesis of CDs from glucose in the presence of alkalis or acids,<sup>67</sup> (iii) thermal decomposition of carbon precursors using non coordinating solvents<sup>68</sup> and (iv) electrochemical carbonization of alcohols under alkaline conditions.<sup>69</sup>

Depending upon the synthesis method and structure, the crystallinity and morphology of carbon dots could be classified into three categories: (i) graphene quantum dots, carbon dots having a  $\pi$  conjugated single layer sheet; (ii) carbon nanodots, amorphous quasi-spherical nanodots having no quantum confinement effect; and (iii) carbon quantum dots, nanodots with a quantum confinement effect and crystalline structure. One can distinguish these above materials based on precursors that are being used in the synthesis procedure. Like in the case of graphene quantum dots (GQDs), the precursors are graphene-based materials while CQDs are synthesized from other crystalline carbon materials like carbon nanotubes.<sup>70</sup> Besides, the excitation wavelength is responsible for the different emission wavelengths and intensity of the carbon dots.<sup>62</sup> Carbon nanodots show some attractive optical properties such as chemiluminescence, electro-chemiluminescence, size-dependent photoluminescence, up-conversion luminescence, and photo-induced electron transfer.<sup>62</sup> CDs generally show evident optical absorption in the UV region with an absorption band around 260–320 nm and this wavelength can be enhanced by surface passivation. CDs have the most promising feature, *i.e.* photoluminescence (PL) emission which contains independent and  $\lambda_{\text{ex}}$ -dependent photoluminescence, and this phenomenon is based on core and surface state-related emission. Zhao and coworkers stated that  $\lambda_{\text{ex}}$ -dependent PL emission depends upon the different sizes of CDs.<sup>63</sup> PL is

measured by a parameter called quantum yield (QY). It has been reported that naked CDs exhibit multicolor fluorescence emission but the QY of these CDs is generally much lower.<sup>71,72</sup> The QY can be enhanced by several approaches such as passivation<sup>73</sup> and purification procedures, and doping with other elements.<sup>74</sup> They have been broadly used for the fluorescence analysis of different targets such as  $\text{H}_2\text{O}_2$ ,<sup>75</sup> ions<sup>76</sup> and macromolecules like proteins due to their outstanding PL properties. Mercury ions are considered as heavy metal ions which may accumulate in vital organs and cause many diseases.<sup>77</sup> Qin and coworkers observed that the PL emission of CDs could be selectively quenched by  $\text{Hg}^{2+}$  ions, and with the help of this phenomenon they synthesized CDs from flour with a detection limit of 0.5 nM.<sup>78</sup> Hydrogen peroxide ( $\text{H}_2\text{O}_2$ ) is a kind of stable reactive oxygen species (ROS) and is involved in signal transduction, cell proliferation, aging, and death.<sup>79</sup> Liu and coworkers prepared nitrogen-doped CD catalyzed Ag nanoparticle (AgNP) composites which could be used to detect the  $\text{H}_2\text{O}_2$  levels with a detection limit of 0.5  $\mu\text{M}$ .<sup>75</sup>

## 2.5. Other carbon-based nanomaterials

In recent decades, a wide range of carbon-based nanomaterials has been studied for the development of various applications, focusing on their attractive electronic properties. Thus, numerous carbonaceous materials have been planned like carbon nanohorns, nanodiamonds, nitrogen vacancy (NV) centre nanodiamonds, nano carbon black and nanofibres. A short explanation of these carbon-based materials is discussed below.

Carbon nanohorns or single-walled nanohorns (SWCNHs) are very related single-walled carbon nanotubes, discovered by Iijima in 1998.<sup>80</sup> SWCNHs usually look like conical carbon structures made up of  $\text{sp}^2$  carbon sheets having a length in the range of 40–50 nm and a diameter of 2–5 nm (Fig. 4A).<sup>81</sup> The structure of single-walled carbon nanohorns can be classified into three different types such as: “bud-like”, “dahlia-like”, and “seed-like”.<sup>82</sup> Nanohorns can show rich and diverse chemistry as the surface of nanohorns consists of a mixture of heptagons, hexagons, and pentagons. Significant quantities of carbon nanohorns could be produced with high purity at room temperature. Besides, there is no use of toxic metal catalysts for the entire process, and to evaluate their biocompatibility, no supplementary clean-up steps are required.<sup>83</sup> They have high conductivity, high dispersibility, excellent chemical and thermal stability, field-emission characteristics and semiconducting properties. As compared to carbon nanotubes, SWCNHs are metal-free and highly purified as well. So they could be used in biosensor studies. SWCNHs were first used to construct a glucose biosensor.<sup>84</sup> The biosensor was manufactured by encapsulating glucose oxidase in the Nafion–SWCNH composite. The glucose biosensor relying on the Nafion–SWCNH composite acquired a low detection limit, high sensitivity, and good selectivity.<sup>84</sup> Later on, SWCNHs were used in the form of a biocompatible and novel matrix for constructing  $\text{H}_2\text{O}_2$  biosensors. Besides this, an electrochemical biosensor has





**Fig. 4** (A) The structure of a carbon nanohorn. (B) Schematic representation of the possible hybridization in nanodiamonds. (C–E) Schematic demonstration of formation of the cup-stacked CNF structure and (F) platelet CNF structure. (B) Reproduced from ref. 86 with permission from the Institute of Physics (IOP), copyright [2016].<sup>86</sup> (A) and (C–F) Reproduced from ref. 81 and 101 with permission from Multidisciplinary Digital Publishing Institute (MDPI), copyright [2021, 2014].<sup>81,101</sup>

been fabricated by adsorbing heme protein myoglobin (Mb) onto the surface of non-covalently functionalized SWCNHs in the presence of poly(styrene sulfonate) (PSS).<sup>85</sup>

Nanodiamonds are carbon nanomaterials with a diamond-like crystal structure constructed from  $sp^3$ -hybridized carbon atoms having diameters in the range of 1 to 20 nm (Fig. 4B).<sup>86,87</sup> Their properties are quite similar to the organic molecules rather than bulk diamonds as the carbon atoms are mostly attached to hydrogen and other non-carbon atoms. Nanodiamonds (NDs) can be prepared in various methods, but the most general method is the detonation process where trinitrotoluene and hexogen explosives are detonated in a controlled oxygen-deficient, high-temperature and high-pressure atmosphere<sup>88</sup> and hence called “detonation NDs”. Nanodiamonds have electrical resistivity and high thermal conductivity and show exceptional mechanical characteristics such as hardness and high strength as well as optical properties like refractive index and high optical transparency.<sup>89</sup> NDs are considered

as a wide-band semiconducting material with the highest optical band gap of all known materials.<sup>90</sup> The exceptional properties of nanodiamonds facilitate their applications in different research areas including electronics, energy, optical computing, and environmental areas. Furthermore, high biocompatibility and low cytotoxicity make NDs a promising material for biosensing applications.<sup>91</sup> The core of nanodiamonds is extremely tailorable and the surface offers some functional groups that can be utilized to modify various systems, such as enzymes and proteins, and also be added into composite materials.<sup>92</sup> Nanodiamonds have offered a unique proposal for bio-conjugation with metalloproteins, DNA, antigens, and enzyme molecules. Recently, researchers developed an enzyme-modified diamond sensor that has been employed for the detection of urea in solutions.<sup>93</sup> Besides this, in the development of an EDIS penicillin sensor, the pH-sensitive properties of O-terminated NDs have also been studied.<sup>93</sup> Nowadays, NV centre nanodiamonds are used as a highly sensitive material





in different types of biosensors. Basically, the NV centre is termed as a point defect of nanodiamonds, consisting of a nitrogen atom which replaces a carbon atom and a vacancy pair along the  $\langle 111 \rangle$  directions.<sup>94,95</sup> Carbon nano black is an extremely fine fluffy powder with a high surface area.<sup>96</sup> This has been a widely used nanomaterial in the biosensing field due to its high surface area and conductivity. Arduini and coworkers have developed a screen-printed electrode modified with carbon black nanoparticles for electrochemical detection of paraoxon.<sup>97,98</sup>

Carbon nanofibers (CNFs) are one of the most important one-dimensional materials of the carbon family that have been explored in both fundamental research and practical applications. Depending upon size, there are some dissimilarities between conventional carbon fibers (CCFs) and carbon nanofibers. The conventional CFs have diameters in the range of micrometers whereas CNFs have diameters in the range of 50–200 nm. CNFs can be synthesized by a less expensive electro-spinning method where the polymer nanofibers are needed to be prepared as they are used as precursors of the CNFs<sup>99</sup> or by the catalytic thermal chemical vapor deposition growth method, generally cup-stacked CNFs and platelet CNFs are synthesized by this method (Fig. 4C–F).<sup>100,101</sup> The performance of CNFs could be increased by the modification of the active surface by adding oxygenated groups. In addition, carbon nanofibers show high absorption capacity, definite surface area, and high porosity. Carbon nanofibers can show the same high conductivity as observed in carbon nanotubes but CNFs can provide an even larger functionalized surface area for the immobilization of biomolecules such as proteins, enzymes, and DNA as compared to carbon nanotubes.<sup>102,103</sup> They can also be easily functionalized due to the presence of oxygen-containing active sites on their surfaces.<sup>102</sup> Therefore, functionalization is a very crucial part of utilizing their unique properties for the development of biosensors. Wu and coworkers introduced a CNF-based amperometric glucose sensor,<sup>104</sup> which confirmed the exceptional catalytic activity of soluble CNFs. On the basis of the electro-catalytic activity of CNFs toward NADH, Arvinte and co-workers reported a CNF-based electrochemical biosensor and the whole electrochemistry of NADH was observed at the CNF modified carbon electrode with a decrease of oxidation potential of more than 300 mV.<sup>105</sup> These studies concluded that CNFs are preferred as an active candidate to construct electrochemical biosensors and sensors.

### 3. Carbon nanomaterial-based biosensor for cancer diagnosis

#### 3.1. Electrochemical biosensor

Among all kinds of biosensors, electrochemical technique-based biosensors are widely used in the diagnosis of diseases, food safety and environmental monitoring. They are a fusion of a biological component with an electronic detection technique.<sup>106</sup> The working principle of these

sensors deals with a specific electrochemical interaction between the surface of the working electrode and the target analyte. The electrochemical responses (current, impedance, potential) are measured when the analyte reacts with the working electrode.<sup>107</sup> Generally, a linear relationship should be maintained between the analyte concentration and sensor response for practical applications. There are different techniques which could be utilized to capture the target molecule; for example, electroactive target molecules, such as dopamine or glucose, can be captured easily with the help of a catalyst or without using a catalyst on the surface of the electrode, and on the other hand, to capture inactive species, other electroactive species such as hexacyanoferrate and hydrogen peroxide ( $\text{H}_2\text{O}_2$ ) are used onto the surface of the electrode. A sandwich-type arrangement of captured analytes activates the redox reaction of electroactive species that enhances the sensitivity of the electrode. The two common things for an electrode used in biosensing are selectivity and sensitivity. The selectivity of an electrode deals with how much specific an electrode is towards a selected target whereas the sensitivity refers to how enhanced electron transfer is from the analyte to the electrode. Increasing the electrode surface area, modifying the electrode by integrating good conducting materials into the electrode, or activating the redox reaction is generally used to increase the electrode response magnitude. Normally, the larger surface area of the electrode has a higher number of reactive sites on it, which results in an increased current response of a target analyte.<sup>108</sup>

In recent years, many techniques have been used to fabricate electrochemical sensors but pencil drawing is one of the attractive, cost-effective and easiest ways for fabricating paper-based devices.<sup>109</sup> The other quantitative part is the limit of detection (LOD), defined as the lowest concentration of analyte where the signal to noise ratio is greater than three, a parameter to check the sensor's performance. In biosensors, selectivity is a crucial part, and depending upon the target material, the bio-recognition element is placed on the electrode element. For cancer sensors, both selection and detection of the target antigen and its concentration in the human body are the main tasks, and therefore the suitable antibody for that particular antigen is placed on the electrode surface.<sup>110</sup> A common DNA biosensor is generally constructed by the immobilization of single-stranded oligonucleotides on sensing substrates to bind with the complementary (target) DNA sequence through hybridization. Then a transducer converts this hybridization into a measurable electrical signal. It is always necessary to stop the nonspecific interactions with the remaining binding site on the electrode surface after immobilization. Based on the surface properties and binding approach, bovine serum albumin (BSA) and thiolated molecules on gold surfaces are broadly used. Carbon nanoparticles (NPs) are ideal components of biosensor platforms due to their excellent electrical properties and large specific surface area. There are so many techniques to synthesize them for biosensor applications.<sup>108,111–113</sup> So far, many electrochemical



approaches have been executed for the detection of cancer biomarkers such as amperometry, voltammetric techniques (cyclic voltammetry (CV), stripping voltammetry, square wave voltammetry, differential pulse voltammetry (DPV), and linear sweep voltammetry) and impedimetry. Among all these techniques, voltammetric methods particularly DPV and CV are usually preferred. In the case of a voltammetric method, two or three-electrode electrochemical cell systems are combined with a potentiostat, which permits the application of potential and measures the obtained current, whereas the working principle of amperometric biosensors includes: (i) an antibody that is attached with an electro-active species like nanoparticles or an enzyme and (ii) this configuration is allowed to capture the target analyte and then (iii) the concentration of the target species or analyte is calculated by applying a certain potential, and the obtained current is measured.<sup>114</sup> The performance of these biosensors depends on the electrode properties as the signal response is produced close to the sensor-electrode surface.

Biomarkers are the most vital part of the diagnosis of any kind of disease. Biomarkers found in body fluids consist of a wide range of materials such as DNAs, RNAs, proteins, polysaccharides, and small molecules (e.g., uric acid, dopamine, and glucose). For cancer biosensors, the detection of antigen concentration is mainly important for cancer diagnosis. Carbon nanomaterials open new pathways for the development of biosensors due to their exceptional mechanical, optical, chemical and thermal properties. Carbon nanomaterials are usually used (i) in the bio-recognition element of the sensor, where they offer binding sites for target biomarkers, (ii) in the transducer section that converts the detected molecular interaction on the electrode surface into an electrochemical signal in the form of current or impedance, and (iii) in labelling for target biomarkers in signal amplification. The surface area of the electrode for immobilization of bio-recognition elements could be increased by functionalizing carbon nanomaterials with organic polymers, biopolymers, and metal oxide nanoparticles. Normally, aptamers, proteins, antigens and antibodies are widely used as biomarker capture probes.<sup>110</sup> The recent development of functional carbon nanomaterials provides new possibilities for improving the performance of electrochemical sensors.

**3.1.1. Graphene-based electrochemical biosensors.** Among all the two dimensional (2D) nanomaterials, graphene, graphene-like materials and graphene-related nanomaterials such as graphene oxide (GO) and reduced graphene oxide (rGO) have been explored to enhance the analytical performance of an electrochemical biosensor in order to detect *in vitro* and *in vivo* cancer biomarkers at an early stage. There are various types of biomarkers that represent different cancer types including nucleic acid biomarkers such as microRNAs (miRNAs), hyper-methylation of the glutathione S-transferase p1 (GSTP1) gene, mutation of the p53 gene, and protein biomarkers such as carcinoembryonic antigen (CEA), alpha-fetoprotein (AFP), cancer antigens (CA125, CA15-3),

and small molecules (dopamine, glucose), which are captured by graphene biosensors due to their high affinity towards these biomarkers. Graphene and related nanomaterial-based electrochemical sensors show rapid response and high selectivity while capturing these nucleic acid biomarkers.<sup>111</sup> A paper-based microfluidic electrochemical platform has been developed by Wu and coworkers using rGO for quantitative analysis of cancer biomarkers.<sup>115,116</sup> Esteban and coworkers developed a screen-printed carbon electrode modified with functionalized *O*-carboxymethylcellulose (CMC) and rGO followed by covalent immobilization with two different selective hairpin-forming capture probes to capture the p53 tumor suppressor (TP53) gene.<sup>117</sup> Furthermore, voltammetric detection of miR-21 from cell lysates of breast and colorectal cancers have also been investigated using a graphene modified electrode. First, passive adsorption of the inosine (In) substituted anti-miR-21 probe occurs onto the surface of a graphene-modified pencil graphite electrode (GME) and then the solid phase hybridization process is placed between the InP probe and the target miR-21 which is monitored by electrochemical techniques such as differential pulse voltammetry (DPV) and electrochemical impedance spectroscopy (EIS) with a detection limit of 2.09 mg mL<sup>-1</sup>. This technique could be used to detect miR-21 in the miR-21 positive breast cancer cell line (MCF-7) compared to the miR-21 negative hepatoma cell line (HUH-7).<sup>118</sup> An electrochemical biosensor was designed by modifying the surface of a glassy carbon electrode with chitosan functionalized rGO to detect vascular endothelial growth factor receptor 2 (VEGFR2) with a detection limit of 0.28 pM and the hybridization event was monitored by a voltammetric technique (Fig. 5).<sup>111</sup> It was observed that the current peak increased while increasing the protein concentration from 0.4 pM to 86 pM. The designed biosensor provided a detection limit of 0.28 pM.<sup>119</sup> This method signifies a simple and effective procedure to measure small changes in target proteins on the electrode surface. A graphene-based electrochemical immunosensor has also been used for the detection of specific tumor biomarkers such as prostate-specific antigen (PSA), carcinoembryonic antigen (CEA), squamous cell carcinoma antigen (SCCA), *etc.* Yang and coworkers designed an immunomagnetic sensor comprising magnetic GO combined with conjugated antibodies of prostate-specific membrane antigen (PSMA) for effective capture and rapid detection of both relevant PSMA and PSMA-positive prostate cancer (PCa) cells in blood samples.<sup>120</sup> A 3-aminopropyl triethoxy saline (APTES) functionalized rGO-zirconia (ZrO<sub>2</sub>) based nanocomposite was also used as a surface modifier for ITO (indium titanium oxide) electrodes to construct biosensors for oral cancer biomarker CYFRA-21-1.<sup>121</sup> Heidari and coworkers proposed a modified glassy carbon electrode (GCE) based immunosensor to detect p53 cancer biomarkers. A sandwich type arrangement of GCE/CdS/p53-Ab1 and a p53-Ab2-tGO-AuNP system have been utilized for the detection of p53 cancer biomarkers. The ECL intensity of the immunosensor



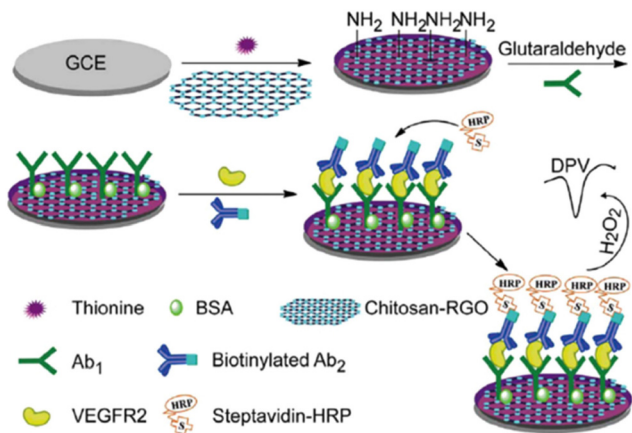


**Fig. 5** Electrochemical detection of vascular endothelial growth factor receptor 2 (VEGFR2) in the presence of a chitosan-rGO based GCE. Reproduced from ref. 111 with permission from Elsevier, copyright [2017].

enhanced due to the fabrication of graphene oxide and gold nanoparticles. The linear range of this immunosensor was found between 20 and 1000  $\text{fg mL}^{-1}$  with a LOD of 4  $\text{fg mL}^{-1}$  for p53 biomarkers.<sup>122</sup> CYFRA21-1 DNA is a sensitive biomarker for non-small cell lung cancer (NSCLC). Chen and coworkers reported a three dimensional electrochemical DNA biosensor for the detection of CYFRA21-1 where ss-DNA probe 5'-SHGAAGGGAGGAATGGTGTTCAGGGGCG-3' is attached onto the Ag nanoparticle functionalized 3D graphene (3D GF/AgNPs). Under optimal conditions, this sensor can detect the target DNA with high sensitivity and with a detection limit of  $1.0 \times 10^{-14}$  M.<sup>123</sup>

### 3.1.2. CNT-based electrochemical biosensors.

Carcinoembryonic antigen (CEA) is a complex, highly glycosylated macromolecule that belongs to the family of cell-surface glycoproteins. The cells of the gastrointestinal tract are responsible for the formation of these glycoproteins during embryonic growth.<sup>124,125</sup> The concentration level of CEA should be lower than 2.5  $\text{ng mL}^{-1}$  in the blood of healthy adults. Ovarian carcinoma, lung and breast cancers,<sup>126</sup> and mainly colorectal carcinoma<sup>127</sup> are associated with the increased concentration level of CEA. Li and coworkers reported label-free electrochemical immunosensing of CEA by a gold nanoparticle (AuNP) functionalized magnetic MWCNT containing Pb(II) modified glassy carbon electrode as a platform for the immobilization of Ab1 to reduce hydrogen peroxide. This sensor provided a linear relationship between the concentration and catalytic reduction of hydrogen peroxide with a detection limit of 1.7  $\text{fg mL}^{-1}$ .<sup>128</sup> Pang and coworkers reported another interesting label-free immunosensor for CEA detection on the basis of ECL properties. They proposed a bio-analytical GCE modified with GO, carboxylated MWCNTs (cMWCNTs) and AuNPs functionalized with cerium oxide nanoparticles ( $\text{CeO}_2$ NPs) dispersed in chitosan. The transduction of the bio-recognition event has been recognized by the decrease in the ECL signals after interaction with CEA, with a detection limit

in the range of 0.02  $\text{ng mL}^{-1}$ . This immunosensor confirmed stability and selectivity (no interference of other biomarkers such as prostatic specific antigen (PSA), BSA, and AFP), with potential application in serum samples (recoveries between 98.9 and 102.6%).<sup>129</sup> A non-enzymatic sandwich-type electrochemical biosensor was introduced where the first antibody (Ab1) of CEA was immobilized on the  $\beta$ -cyclodextrin/multiwalled carbon nanotubes ( $\beta$ -CD/MWCNTs), which improved the electrode surface and enhanced the electrical conductivity (Fig. 6A). Further upgradation of the surface could be achieved by using Ab2 immobilized silver nanoparticles-carbon nanotubes/manganese dioxide ( $\text{Ag NPs-MWCNTs/MnO}_2$ ), which enhanced the electrical conductivity by the catalytic reduction of hydrogen peroxide (Fig. 6B), with a detection limit of 0.03  $\text{pg mL}^{-1}$  for CEA.<sup>130</sup> Heydari-Bafrooei and Shemszadeh prepared an ultrasensitive label-free electrochemical aptasensor based on a modified rGO-MWCNT with densely packed gold nanoparticle (rGO-MWCNT/AuNP) platform to detect the biomarker prostate-specific antigen (PSA) in serum. The detection was carried out on the variation of electron transfer resistance ( $R_{ct}$ ) and differential pulse voltammetry (DPV). As compared to other platforms, the rGO-MWCNT/AuNP nanocomposite modified electrode is the most sensitive aptasensing proposal for the determination of PSA with a detection limit of 1  $\text{pg mL}^{-1}$ .<sup>131</sup> In the case of liver cancer diagnosis, capturing the alpha-fetoprotein (AFP) biomarker is the important task to do. Wang and coworkers introduced a label-free AFP immunosensing platform based on a Prussian blue (PB) film-modified GCE covered with SWCNTs functionalized with polylysine (PLL-SWCNTs) to immobilize  $\alpha$ -fetoprotein antibodies (anti-AFP) labeled with horseradish peroxidase (HRP). The sensing was detected by voltammetric and impedimetric techniques with a detection limit of 0.011  $\text{ng mL}^{-1}$ .<sup>132</sup> Li and coworkers developed MWCNT-modified glass carbon electrodes where the surface of the electrode was immobilized with synthetic DNA probes by covalent cross-linking. The probes being complementary with miRNA-24 were hybridized with different concentrations of miRNA-24. The formed hybrids on the electrode surface were estimated by differential pulse voltammetry. The hybridization between the probes and miRNA-24 was detected on the basis of the change of the guanine oxidation signal.<sup>133</sup> Sabahi and coworkers designed an FTO-based biosensor to detect the miR-21 biomarker which is used for the diagnosis of prostate cancer. Here a fluorine-doped tin oxide (FTO) electrode is modified with thiolated receptor probe-functionalized dendritic gold nanostructures (den-Au) which are placed on a single-walled carbon nanotube (SWCNT) platform. The differential pulse voltammetry (DPV) technique is used for the sensing with a detection limit of 0.01  $\text{fmol L}^{-1}$ .<sup>134</sup> Luo and coworkers developed an enzyme free electrochemical immunosensor made up of a SWCNT@GQD composite platform modified with an rGO-AuNP system for the detection of CEA. This immunosensor showed dual-signal amplification results having a linear



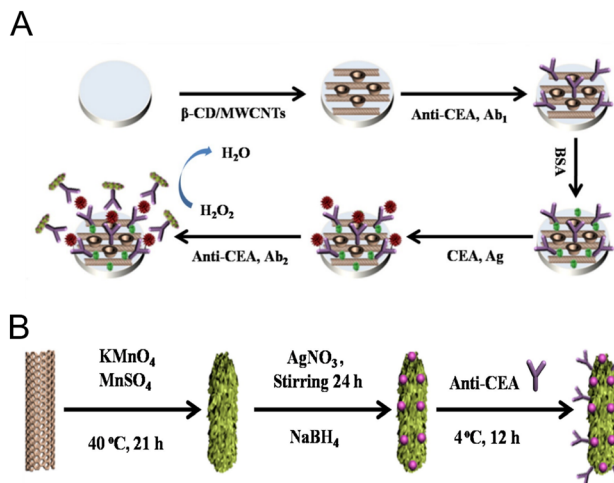


Fig. 6 (A) Synthesis process of the label of a secondary antibody. (B) Schematic representation showing the fabrication process of the immunosensor. Reproduced from ref. 130 with permission from Elsevier, copyright [2017].<sup>130</sup>

range of 50–650 pg mL<sup>-1</sup> with a lower detection limit of 5.3 pg mL<sup>-1</sup>.<sup>135</sup> A genosensor is very cost effective in detection of the colorectal cancer biomarker CEACAM5. In this genosensor, vertically aligned multi-walled carbon nanotubes are placed over a flexible PET substrate by a hot press technique, which is used as a sensing electrode, and then the DNA probe is immobilized to capture the target DNA. Electrochemical impedance spectroscopy (EIS) and cyclic voltammetry were used for the characterization of this biosensor. The hybridization performance was monitored by adding different concentrations of target DNA within a range of 50 to 250 μM and a detection limit was found to be 0.92 μM.<sup>136</sup> Nowadays, in all newly diagnosed cases, it has been observed that non-small cell lung cancer (NSCLC) is the most common type of lung cancer. Mei and coworkers designed an ultrasensitive electrochemical biosensor where a gold nanocage and amidated multi-walled nanotube (Au NC/MWCNT-NH<sub>2</sub>) modified screen printed electrode has been used for the detection of MALAT1, a diagnostic biomarker of NSCLC. Cyclic voltammetry was used for the sensing with a low detection limit of 42.8 fM.<sup>137</sup>

**3.1.3. Carbon quantum-dot-based electrochemical biosensors.** The application of carbon quantum-dots (QDs) in the development of biomarker sensors is now in its early stage.<sup>112</sup> Generally, graphene QDs are considered to date as a potential candidate for the construction of ECL and fluorescence-based biosensors. Wu and coworkers developed a label-free ECL immunosensor with a detection limit of 0.29 pg mL<sup>-1</sup> for the detection of PSA by coating Au/Ag-rGO, modified with amidated GR-QDs and GO-QDs, onto a GCE and immobilizing anti-PSA on the electrode surface.<sup>138</sup> Li and coworkers constructed a highly sensitive paper-based ECL immunobiosensor for the detection of CEA by using nanoporous gold–chitosan hybrids and graphene quantum dot functionalized Au@Pt.<sup>139</sup> The one-pot simple synthetic

strategy of graphene quantum dots shows a higher quantum yield and higher biocompatibility. With the property of good conductivity, Yang and coworkers developed an ECL based technique for the detection of tumor marker carbohydrate antigen 199 (CA199), by modifying a GCE with Au and Ag NP functionalized rGO which enhanced the surface area of the electrode to capture a large number of primary antibodies (anti-CA199). The signal amplification has been done by anti-CA199 immobilization on GO-QD modified PtPd nano chains. Under optimal conditions, the ECL immunosensor displayed a higher detection range of 0.002–70 U mL<sup>-1</sup> and a lower detection limit of 0.96 mU mL<sup>-1</sup>.<sup>140</sup> A sensitive and accurate method has been developed for the determination of miRNA-155 by constructing an electrochemical biosensor, where activated carboxyl groups of graphene quantum dots (GQDs) assembled on the aminated DNA structure were immobilized onto the surface of the electrode. A certain amount of HRP (horseradish peroxidase) immobilized on GQDs which helped to enhance the electrochemical signals by effectively catalyzing the hydrogen peroxide (H<sub>2</sub>O<sub>2</sub>)-mediated oxidation of 3,3',5,5'-tetramethylbenzidine (TMB). The proposed electrochemical sensor displayed detection range of 1 fM to 100 pM with a LOD value of 0.14 fM.<sup>141</sup> Serafin and coworkers reported the development of the first integrated electrochemical immunosensor to detect IL-13Rα2. The working function of this sensor is based on two parts; one of which is GQD functionalized MWCNTs as nanocarriers of multiple detector antibodies and HRP molecules and the other one is biotinylated capture antibody of IL-13Rα2, immobilized on the streptavidin-modified screen-printed electrodes (Fig. 7). A linear calibration plot varies from 2.7 to 100 ng mL<sup>-1</sup> of IL-13sRα2 observed in the amperometric detection of a H<sub>2</sub>O<sub>2</sub>/hydroquinone (HQ)b system with a LOD value of 0.8 ng mL<sup>-1</sup>.<sup>142</sup> Selective mutation in the BRCA1 gene, responsible for breast cancer, could be recognized by a DNA biosensor based on the interaction of DNA layers attached onto a carbon nanodot modified gold electrode (CD/AuSPE) and thionine. Here, a probe (PROBEBRCA1) was first immobilized onto the electrode and the recognition of target ssDNA and detection of a mutation were based on the hybridization event which was monitored using thionine as a redox indicator and DPV. Under optimal conditions, this DNA sensor displayed a detection limit of 55 pg mL<sup>-1</sup>.

### 3.2. Optical biosensor

The working mechanism of these sensors deals with the changes occurring in the emission of light considering different target-recognition element interactions. A signal is generated by the optical biosensor which is proportional to the amount of target analyte present. Carbon NPs, especially graphene derivatives, come under the prominent fluorescence quenchers.<sup>143</sup> A GO or rGO-based fluorescence sensor is generally based on a fluorophore covalently bound to a target capture probe which may be adsorb non-covalently onto GO, but removed from the GO surface when the target is attached. Adsorption leads to the quenching of fluorescence, but is re-established upon target-capture probe



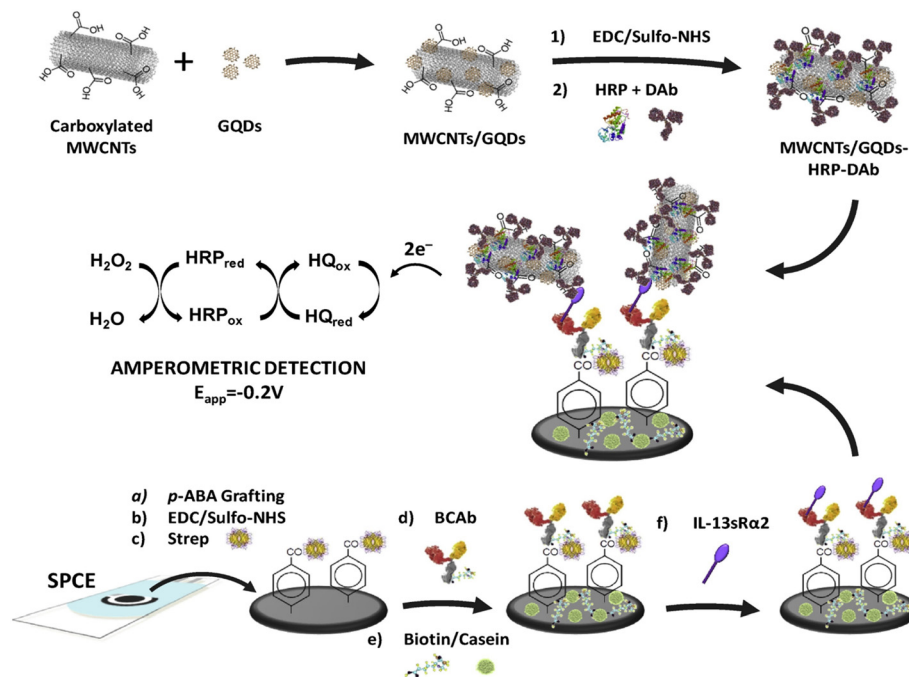


Fig. 7 Scheme for the detection of IL-13sR $\alpha$ 2 by a sandwich amperometric immunosensor using MWCNT/GQD-HRP-DAb nanocarriers. Reproduced from ref. 142 with permission from Elsevier, copyright [2017].<sup>142</sup>

interaction.<sup>110</sup> Due to some effective factors such as high signal intensity, low background noise, easy detection, and multiple target detection capability, these optical biosensors including surface-enhanced Raman scattering (SERS), surface plasmon resonance (SPR), and localized surface plasmon resonance (LSPR) are very promising for bioassay application.<sup>143</sup>

**3.2.1. Graphene based optical biosensor.** In SPR based sensors, biorecognition elements are immobilized onto the metal surface for molecular interaction with the target analyte or biomarker and the interaction leads to a change in mass and the refractive index of the sensor surface layer. The transducer converts this interaction into an SPR signal as a result of the concentration of analyte.<sup>144</sup> A very sensitive and simple SPR biosensor has been constructed for the detection of miRNA-141 by using graphene oxide-gold nanoparticle (GO-AuNP) hybrids. Taking advantage of better performance by GO-AuNP hybrids in SPR biosensors, the detection of miRNA was achieved in two steps; firstly, the surface of the Au film was immobilized by a short complete complementary sequence of the thiolated capture DNA probe to recognize the sequence of target miRNA-141 and secondly, the other sequence of miRNA-141 was captured by the assistant DNA-linked GO-AuNP hybrids. It was observed that the constructed SPR biosensor presented a detection limit as low as 1 fM.<sup>145</sup> A numerical analysis of the graphene-coated fiber-optic based SPR biosensor has been developed to identify the early onset of breast cancer gene-1 (BRCA1) and breast cancer gene-2 (BRCA2). 916delTT and 6174delT are two specific mutations observed in BRCA1 and BRCA2, considered for numerical detection of breast cancer. The hybridization event

of DNA along with individual point mutations in BRCA1 and BRCA2 genes was monitored by the attenuated total reflectance technique.<sup>146</sup> Carboxyl-functionalized graphene oxide (GO-COOH) on the Au film surface is a highly efficient material for the SPR based biosensor to detect non-small cell lung carcinoma (NSCLC) using the cytokeratin-19 (CK19) protein biomarker. It has been observed that the field energy propagation intensity and sensitivity for the detection of CK19 protein by an SPR can be enhanced by depositing -COOH modified GO sheets compared to other conventional Au-based SPR chips and the lowest detectable limit was as low as 1 fg mL<sup>-1</sup>.<sup>147</sup> Li and coworkers developed a selective and sensitive label free graphene-based SPR biosensor for the determination of folic acid protein (FAP) at the fM level in human serum.<sup>148</sup> Depending upon the polarization and absorption of graphene under total internal reflection, Fei and coworkers developed a graphene-based optical refractive index sensor in high resolution of  $1.7 \times 10^{-8}$  with  $4.3 \times 10^7$  mV per RIU sensitivity, as well as a wide dynamic range. This high sensitivity of the graphene optical sensor could be utilized for live-cell, non-labeled and exact detection of less concentrated cancer cells among normal cells at the single-cell level. Besides this, it can show simultaneous detection and discrimination of two cell lines without separation.<sup>149</sup> An exclusive optical method that has a direct connection with cancer diagnosis is the detection of the concentration level of a cancer biomarker, pyrophosphate (PPi). Enhancement in selectivity and sensitivity of PPi detection could be achieved by the fabrication of the fluorescent probe PDI-HIS, copper ions, and graphene oxide (GO). Under optimal experimental conditions, the proposed sensor platform which is a self-



assembled nanocomposite made of PCG (PDIHis + GO + Cu<sup>2+</sup>) showed a low detection limit of 1 fM for PPI compared to PDI-HIS-Cu<sup>2+</sup>.<sup>150</sup>

**3.2.2. Carbon nanotube based optical biosensors.** Single-walled carbon nanotubes (SWCNTs) exhibit near-infrared (NIR) photoluminescence (fluorescence) properties that has been explored in field biosensing applications. These fluorescence properties are observed in the 900–1600 nm range. Ryan M. Williams and coworkers developed a sensitive and specific fluorescent biosensor by using the optical properties of carbon nanotubes for the detection of the metastatic prostate cancer biomarker urokinase plasminogen activator (uPA). Photoluminescent SWCNTs were modified to specifically respond to uPA *via* antibody conjugation. Due to this conjugation, modulation of the optical bandgap is controlled by the analyte interaction.<sup>151</sup> The DNA/aptamer-CNT platform showed better results for the detection of cancer biomarker CA125. A fluorescent biosensor has been reported for the detection of the CA125 biomarker using anti-CA125 antibody immobilized three-dimensional carbon nanotubes (3DNCNTs).<sup>152</sup>

The near-infrared emission, photostability and sensitivity of SWCNTs make them a perfect candidate for the development of optical sensors. CNT-based sensors are capable of real-time optical measurement of hybridization actions of microRNA and other oligonucleotides. A DNA-nanotube based photoluminescent biosensor was developed with a (GT)<sub>15</sub> single oligonucleotide sequence for the detection of mir19 and R23 RNA. The single oligonucleotide sequence has two parts, a nanotube binding sequence and a miRNA capture sequence. The detection limit ranged from 10 and 100 pM (0.5–5 fmol) at a low concentration level of sensor of 0.02 mg l<sup>-1</sup>.<sup>153</sup> Chronic myeloid leukemia (CML) is one type of blood cancer and the early diagnosis is very much important for the survival of the patients. A light-induced optical biosensor containing CNTs is used as an electrooptic material, which can detect leukemia, K562 cells. 3-Glycidoxypropyl trimethoxysilane (GPMS) molecule functionalized CNTs are used as a sensing platform, immobilized with P-glycoprotein (anti-P-gp), and the detection of leukemia K562 cells is based on charge transfer induced Fermi level fluctuation of the electrode which in turn is calculated in terms of the photoconductive response, with a detection limit of 27 cells per ml.<sup>154</sup> Prostate-specific membrane antigen (PSMA) is a glycoprotein developed in the prostatic epithelium, which is used as a biomarker for the early detection of prostate cancer.<sup>155</sup> Juzgado and coworkers reported a specific and sensitive novel ECL ELISA-like immunosensor based on carbon nanotubes along with a highly specific sandwich type immunoassay for the detection of PSMA. To engineer the device, an optically transparent electrode was tailored with doubly functionalized MWCNTs containing amine groups and a monoclonal anti-PSMA antibody and the antibody was labeled with an ECL probe. Under experimental conditions, the proposed sensing device presented a LOD of 0.88 ng mL<sup>-1</sup> in real complex samples

such as cell lysates.<sup>156</sup> Exosomes are also considered as a cause of cancer. Exosomes can be detected by a visible and colorimetric aptasensor based on DNA capped SWNTs. Aptamers immobilized onto the surface of SWNTs are bound with the exosome's transmembrane protein CD63 (Fig. 8A) and leave the surface through conformational changes which efficiently catalyze H<sub>2</sub>O<sub>2</sub>-mediated oxidation of 3,3',5,5'-tetramethylbenzidine (TMB) and change its colour to blue in solution. Under optimized experimental conditions, the LOD is in the range of 5.2 × 10<sup>5</sup> particles per μL.<sup>157</sup> Yong and coworkers developed a novel CNT-based multicolor fluorescent peptide nanoprobe considering the sensitivity and rapid response towards the detection of three cancer-related proteases such as matrix metalloproteinase-7 (MMP-7), uPA and matrix metalloproteinase-2 (MMP-2). The C-terminal of each of these three probes is labeled with a fluorescent dye (*i.e.* cyanine dye Cy3, fluorescein isothiocyanate (FITC), cyanine dye Cy5) to react with three different probes conjugated to the surface of CNTs. The detection of this protease by nanoprobe is based on the fluorescence quenching properties of the dye *i.e.* highly efficient long-range energy transfer from the dyes to CNTs. Besides this, selective peptide cleavage occurred upon incubation with the target proteases and released the dye from the surface of the CNTs, which results in fluorescence recovery that gives the source for the quantitative measurement of protease activity (Fig. 8B). The reported LOD for this method is 0.5 pg mL<sup>-1</sup> to 500 pg mL<sup>-1</sup>.<sup>158</sup>

**3.2.3. Carbon nanodot based optical biosensor.** CQDs have attracted huge attention due to their numerous favorable features including chemical inertness, small size, low toxicity and eco-friendliness, size dependent luminescence emission, biocompatibility and water solubility.<sup>62,65,159</sup>

CQDs are used as a useful fluorescent probe platform for miRNA detection. The adsorption of FAM-labeled ss-DNA on carbon quantum dots through π-π interactions resulted in quenching of the fluorescence intensity when it binds to miR9-1. Fluorescence resonance energy transfer (FRET) from dyes to CQDs resulted in quenching of fluorescence. A duplex helix was formed and double-stranded DNA/miRNA was released from the surface of CQDs when miR9-1 binds with the FAM-labeled ss-DNA and the fluorescence intensity was recovered.<sup>160</sup> Early diagnosis has great practical significance for the survival and treatment of cancer patients. Shuaimin Lu and coworkers constructed a novel and ultra-sensitive fluorescent biosensor for the detection of tumor invasive biomarker β-glucuronidase (GLU) which is based on the inner-filter effect (IFE). Nitrogen-doped CQDs (N-CQDs) were synthesized and due to the presence of green photoluminescence properties, they were employed as the fluorophore in the IFE. 4-Nitrophenyl-β-D-glucuronide (PNPG) was used to perform as the GLU substrate, and the GLU catalytic product *p*-nitrophenol (*p*NP) was able to act as the strong absorber in the IFE to quench the fluorescence of N-CQDs due to the corresponding overlap between the absorption of *p*NP and the excitation of N-CQDs. The signal





**Fig. 8** (A) Principle of the DNA capped single walled carbon nanotube (SWNT)-based aptamer biosensor. Reproduced from ref. 157 with permission from Elsevier, copyright [2017].<sup>157</sup> (B) The principle of the MWCNT-based multicolor fluorescent peptide nanoprobe for the multiplex detection of MMP-7, MMP-2, and uPA. Reproduced from ref. 158 with permission from The Royal Society of Chemistry, copyright [2013].<sup>158</sup>

of the GLU activity could be monitored by the fluorescence intensity of N-CQDs. This method presented a low detection limit of  $0.3 \text{ U L}^{-1}$ .<sup>161</sup> Identification of carbohydrate antigen 15-3 (CA15-3), an important breast cancer biomarker, has been done by a sandwich type chemiluminescence immunosensor, where a graphene oxide-PEI-carbon quantum dot (CQD)-Au nanohybrid acts as a probe. Here, an

Au and poly-dopamine based nanocomposite surface provided a higher surface for immobilization of the initial antibody (Ab1) which targets CA15-3 and the secondary antibody (Ab2) was immobilized by an AuNP/CQD-PEI-GO composite which acts as a nanoprobe (Fig. 9). Under the synergistic action of polydopamine, AuNPs, PEI-GO and AgNPs, the ECL signal of CQDs was significantly enhanced



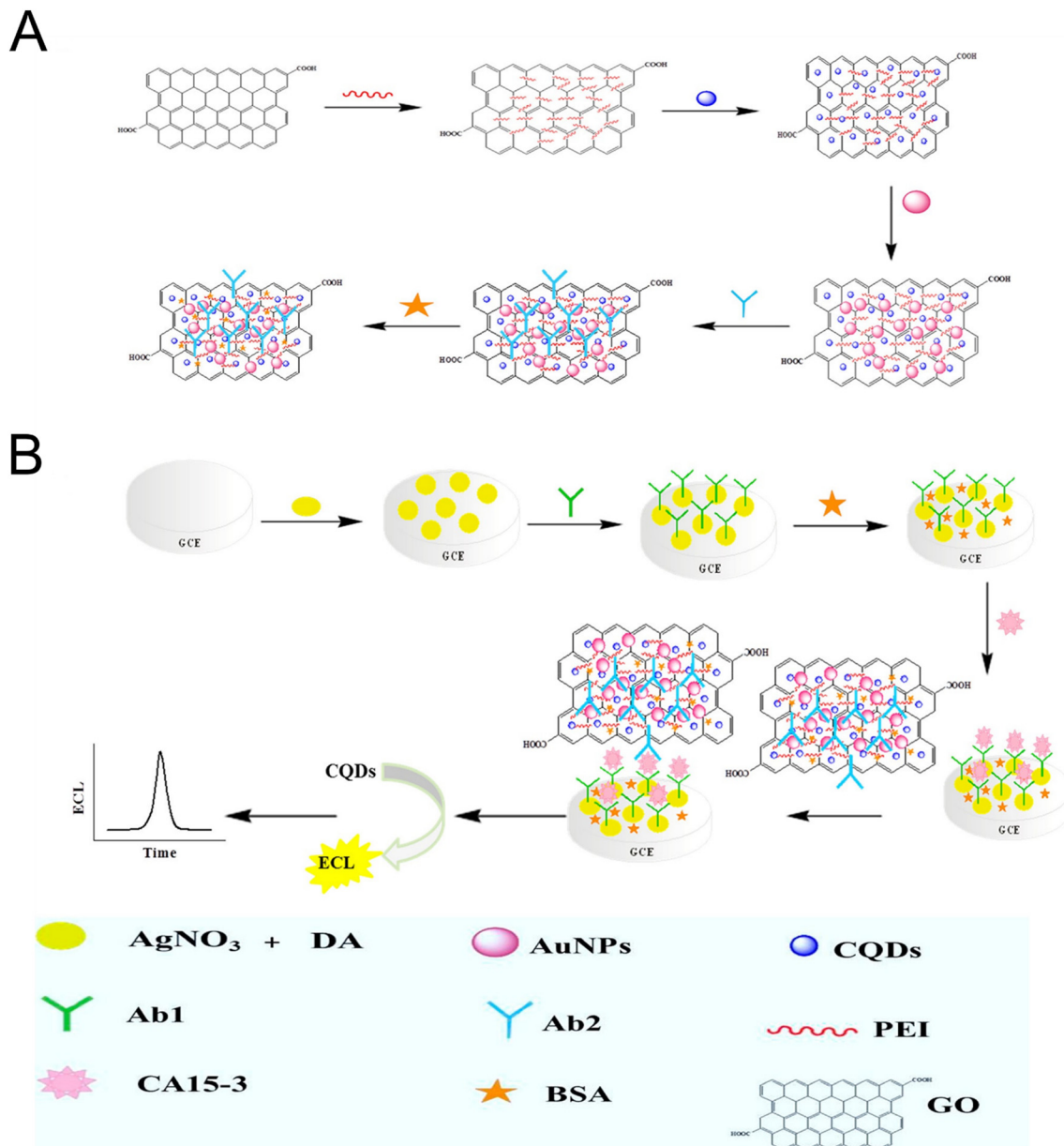


**Fig. 9** (A) Schematic representation of immobilization of AuNP Ab2 and CQDs on the PEI-GO matrix. (B) Fabrication process of the proposed ECL immunosensor. Reproduced from ref. 162 with permission from the American Chemical Society (ACS), copyright [2019].<sup>162</sup>

and considered as an excellent conductive material to speed up the electron transfer rate and electrochemical detection capability as well. Under optimal conditions, the constructed immunosensor presented a linear concentration in the range from 0.005 to 500 U mL<sup>-1</sup>, with a detection limit of 0.0017 U mL<sup>-1</sup>.<sup>162</sup> Meng and coworkers developed a new ECL biosensor for ultrasensitive and selective determination of K562 leukemia cells. In order to develop the platform, a screen-printed carbon electrode was modified with nonporous gold. The good biocompatibility and less cytotoxicity of the carbon quantum dot (CQD) coated ZnO nanosphere (ZnO@CQD) system made it a good ECL label. The aptamer was introduced to capture the cells and a concanavalin A conjugated ZnO@CQD system was used for

selective hybridization with the cell surface carbohydrate. The proposed scheme exhibited excellent analytical performance having a detection limit of 46 cells per mL.<sup>163</sup> Mohammadi and coworkers engineered a FRET sensing platform for the quantification of miRNA-155 with the help of CDs and MnO<sub>2</sub> nanosheets, acting as energy donor-acceptor pairs. The proposed sensing system showed high specificity and was able to differentiate between complementary target miRNA-155 and single base mismatch miRNA-155. This approach has been taken into account in order to detect not only spiked serum samples but also breast cancer cells such as MCF-7.<sup>164</sup> Ding and coworkers designed an aptasensor where they used a FRET pair made up of graphene oxide (GO) and an MUC1 aptamer conjugated





carbon dot (aptamer-CDs) system for the identification of the Mucin-1 (MUC1) protein. The FRET process takes place between aptamer-CDs and GO *via* specific  $\pi$ - $\pi$  interaction. Despite addition of the target MUC1 protein, the competitive attraction between aptamer-CDs and MUC1 is always greater than that of aptamer-CDs and GO. As a result, the aptamer-CDs were removed from the GO surface and the fluorescence intensity of the CDs was restored. The linearity of this aptasensor was achieved in the range of 20.0–804.0 nM with a detection limit of 17.1 nM.<sup>165</sup> Mintz and coworkers developed an assay by combination of AuNPs and CDs for  $\alpha$ -L-fucosidase (AFU) biomarker detection to monitor hepatocellular carcinoma (HCC). The selective interaction between AFU and its corresponding antibody (IgG anti-FUCA2) activates the fluorescence quenching properties of CDs through energy transfer to the surface plasmon band of the AuNPs, when they are present in close proximity in the presence of AFU. According to this proposed assay, a detection limit of 3.4 nM and a broad linear detection range from 11.3 to 200 nM could be achieved.<sup>166</sup> A CD based heterogeneous immunoassay was constructed for the detection of human  $\alpha$ -fetoprotein (AFP) using “nanolight CDs” with a solid-phase platform. This immunoassay was based on a sandwich immune complex made between CD labeled Ab2 and AFP bound to the Ab1, immobilized onto polystyrene well plates. The fluorescence intensities of this sandwich immunosorbent assay were proportional to the AFP antigen concentrations.<sup>166</sup>

#### 4. Conclusion and future prospects

Nanomaterials are usually applied for surface modification of working electrodes. Besides increasing the electrode's effective surface area, they also enhance the performance of the electrode. Surface modification with nanomaterials also helps to amplify the output signals of a particular biosensor by increasing the speed of electron transfer across electrode/solution interfaces. The unique characteristics of carbon nanomaterials have comprehensively contributed to the growth and evolution of biosensors for the diagnosis of cancer. As compared to other conventional sensing techniques, carbon nanomaterial-based novel biosensors exhibit better analytical performance. The unique properties of graphene, CNTs, nanohorns, carbon nanodots, and nanodiamonds have been proving different points of view in the construction of novel nanostructured biosensors. In the last few years, significant efforts have been made for the advancement of immuno- and DNA-biosensors to determine the prominent cancer biomarkers. Considering the features of cost effectiveness, sensitivity, stability, simplicity and selectivity, carbon nanostructure-based biosensors are potential tools for the development of novel diagnostic technologies. In reality, with the advancement in nanotechnology, mostly in the field of carbon-based nanomaterial synthesis and production, the contribution of such materials also increases in the development of the

biosensing field. Biosensing electrodes modified with nanostructures improve not only the performance of electrochemical and optical properties, but also a suitable and biocompatible atmosphere for the immobilization of recognition elements has been achieved, which is an important step to set up immuno- and DNA-biosensors. Thus, in this review, we presented a critical discussion about different types of carbon nanomaterial based-biosensors for the clinical diagnosis of cancer which have been reported in the last few decades, highlighting the benefits of using carbon nanostructured materials in the different stages during the construction of biosensors. The biosensors discussed in this article offer highly selective, cost-effective and sensitive detection of cancer biomarkers with the help of carbon nanomaterials as components. Therefore, the biosensors would be extensively useful as an important element for the advancement of automated diagnostic systems. To achieve this goal, the main parameters of biosensors like reproducibility, stability and biocompatibility should be further improved in order to make them useful in clinical laboratories and hospitals for the purpose of low-cost diagnosis.

#### Abbreviations full form

CSF	Cerebrospinal fluid
BCSCs	Breast cancer in stem cells
Apo-A1	Apolipoprotein-A1
ELISA	Enzyme-linked immunosorbent assay
IHC	Immunohistochemistry
PCR	Polymerase chain reaction
HPLC	High-performance liquid chromatography
RIA	Radioimmunoassay
POC	Point of care
NiHCFNPs	Nickel hexacyanoferrate nanoparticles
CDs	Carbon dots
GQDs	Graphene quantum dots
SWNTs	Single walled nanotubes
MWNTs	Multi-walled nanotubes
CNTs	Carbon nanotubes
GIC	Graphitic intercalation compounds
GO	Graphene oxide
CVD	Chemical vapor deposition
FET	Field-effect transistor
BPE	Bipolar electrode
PSA	Prostate-specific antigen
DWNTs	Doubled-walled carbon nanotubes
IP	Ionization potential
EA	Electron affinity
C-dots	Carbon dots
PL	Photoluminescence
QY	Quantum yield
ROS	Reactive oxygen species



AgNPs	Ag nanoparticles	anti-AFP	A-fetoprotein antibody
H <sub>2</sub> O <sub>2</sub>	Hydrogen peroxide	FTO	Fluorine-doped tin oxide
SWCNHs	Single-walled nanohorns	den-Au	Dendritic gold nanostructures
Mb	Myoglobin	EIS	Electrochemical impedance spectra
PSS	Polystyrene sulfonate	PET	Polyethylene terephthalate
ND	Nanodiamond	NC	Nanocage
EDIS	Electrolyte-diamond-insulator-semiconductor	Au NCs/MWCNT-NH <sub>2</sub>	Gold nanocages/amidated multi-walled nanotubes
CNFs	Carbon nanofibers	MALAT1	Metastasis-associated lung adenocarcinoma transcript 1
CCFs	Conventional carbon fibers	CA	Carbohydrate antigen
NADH	Nicotinamide adenine dinucleotide hydride	GR-QDs	Graphene reduced quantum dots
LOD	Limit of detection	GO-QDs	Graphene oxide quantum dots
BSA	Bovine serum albumin	TMB	3,3',5,5'-Tetramethylbenzidine
NP	Nanoparticle	HQ	Hydroquinone
CV	Cyclic voltammetry	IL-13R $\alpha$ 2	Interleukin-13 receptor subunit alpha-2
DPV	Differential pulse voltammetry	SPE	Screen-printed electrode
DNA	Deoxyribonucleic acid	ssDNA	Single stranded DNA
RNA	Ribonucleic acid	BRCA1	Breast cancer type 1 susceptibility protein
GSTP1	Glutathione S-transferase P1	SPR	Surface plasmon resonance
miRNAs	MicroRNAs	LSPR	Localized surface plasmon resonance
CEA	Carcinoembryonic antigen	SERS	Surface-enhanced Raman scattering
AFP	Alpha-fetoprotein	GO-AuNPs	Graphene oxide-gold nanoparticles
CMC	Carboxymethylcellulose	BRCA2	Breast cancer gene-2
RGO	Reduced graphene oxide	ATR	Attenuated total reflection
InP	Inosine substituted probe	GO-COOH	Carboxyl-functionalized graphene oxide
GME	Graphene modified electrode	CK19	Cytokeratin 19
EIS	Electrochemical impedance spectroscopy	FAP	Folic acid protein
HUH-7	Hepatoma cell line	mV	Millivolt
VEGFR2	Vascular endothelial growth factor receptor 2	PPI	Pyrophosphate
SCCA	Squamous cell carcinoma antigen	PDI-HIS	Histidine functionalized perylenediimide
PSMA	Prostate-specific membrane antigen	uPA	Urokinase plasminogen activator
PCa	Prostate cancer	3DNCNTs	Three-dimensional carbon nanotubes
APTES	Aminopropyl triethoxy saline	CML	Chronic myeloid leukemia
ITO	Indium titanium oxide	GPMS	3-Glycidoxypropyl trimethoxysilane
ZrO <sub>2</sub>	Zirconia	P-gp	P-Glycoprotein
CYFRA-21-1	Cytokeratin 19 fragment	MMP-7	Matrix metalloproteinase-7
GCE	Glassy carbon electrode	MMP-2	Matrix metalloproteinase-2
Ab1	Primary antibody	FITC	Fluorescein isothiocyanate
Ab2	Secondary antibody	CQDs	Carbon quantum dots
AuNPs	Gold nanoparticles	GLU	Glucuronidase
ECL	Electrochemiluminescence	IFE	Inner-filter effect
NSCLC	Non-small cell lung cancer	N-CQDs	Nitrogen-doped carbon quantum dots
tGO	Thiol-functionalized GO	PNPG	4-Nitrophenyl- $\beta$ -D-glucuronide
cMWCNTs	Carboxylated multi-walled carbon nanotubes	PNP	<i>p</i> -Nitrophenol
CeO <sub>2</sub> NPs	Cerium oxide nanoparticles	ZnO	Zinc oxide
$\beta$ -CD/MWCNTs	$\beta$ -Cyclodextrin/multiwalled carbon nanotubes	PEI-GO	Poly(ethylenimine) functionalized graphene oxide
Ag NPs-MWCNTs/MnO <sub>2</sub>	Silver nanoparticles-carbon nanotubes/manganese dioxide	HCC	Hepatocellular carcinoma
Rct	Electron transfer resistance	AFU	A-L-fucosidase
PB	Prussian blue		
HRP	Horseradish peroxidase		



MUC1                            Mucin 1  
MnO<sub>2</sub>                            Manganese dioxide

## Author contributions

SD, BS, MT and DT contributed to the preparation of the manuscript. MT and DT proposed the content, SD, DT and MT proofread the manuscript, contributed to all sections and revised and finalized the text, figures, and tables. All authors read and approved the final manuscript.

## Conflicts of interest

The authors declared no conflict of interest.

## Acknowledgements

DKT thanks the Department of Biotechnology, Govt. of India for the Ramalingaswami Re-entry Fellowship and the University Grant Commission, India for the Faculty Recharge Position at Goa University. Manisha Tiwari thanks the Department of Biotechnology, Govt. of India, for the BioCARE Women Scientist Fellowship.

## References

- 1 S. Pandey, *Biosensors*, 2022, **12**, 219.
- 2 M. Barani, M. Mukhtar, A. Rahdar, S. Sargazi, S. Pandey and M. Kang, *Biosensors*, 2021, **11**, 55.
- 3 S. A. Soper, K. Brown, A. Ellington, B. Frazier, G. Garcia-Manero, V. Gau, S. I. Gutman, D. F. Hayes, B. Korte and J. L. Landers, *Biosens. Bioelectron.*, 2006, **21**, 1932–1942.
- 4 J. Zhao, Y. Tang, Y. Cao, T. Chen, X. Chen, X. Mao, Y. Yin and G. Chen, *Electrochim. Acta*, 2018, **283**, 1072–1078.
- 5 S.-E. Kim, Y. J. Kim, S. Song, K.-N. Lee and W. K. Seong, *Sens. Actuators, B*, 2019, **278**, 103–109.
- 6 H. M. Fahmy, E. S. Abu Serea, R. E. Salah-Eldin, S. A. Al-Hafiry, M. K. Ali, A. E. Shalan and S. Lanceros-Méndez, *ACS Biomater. Sci. Eng.*, 2022, **8**, 964–1000.
- 7 S. Hassanpour, M. Hasanzadeh, A. Saadati, N. Shadjou, J. Soleymani and A. Jouyban, *Microchem. J.*, 2019, **146**, 345–358.
- 8 P. Naderi and F. Jalali, *J. Electrochem. Soc.*, 2020, **167**, 027524.
- 9 T. Zhang, X. Du and Z. Zhang, *Front. Bioeng. Biotechnol.*, 2022, **10**, 993015.
- 10 X. Zhang, Q. Guo and D. Cui, *Sensors*, 2009, **9**, 1033–1053.
- 11 O. N. Oliveira Jr, R. M. Iost, J. R. Siqueira Jr, F. N. Crespilho and L. Caseli, *ACS Appl. Mater. Interfaces*, 2014, **6**, 14745–14766.
- 12 T. Tieu, M. Alba, R. Elnathan, A. Cifuentes-Rius and N. H. Voelcker, *Adv. Ther.*, 2019, **2**, 1800095.
- 13 Y.-R. Yuan, R. Yuan, Y.-Q. Chai, Y. Zhuo and X.-M. Miao, *J. Electroanal. Chem.*, 2009, **626**, 6–13.
- 14 M. S. Mauter and M. Elimelech, *Environ. Sci. Technol.*, 2008, **42**, 5843–5859.
- 15 M. Li, T. Chen, J. J. Gooding and J. Liu, *ACS Sens.*, 2019, **4**, 1732–1748.
- 16 I. Khan, K. Saeed and I. Khan, *Arabian J. Chem.*, 2019, **12**, 908–931.
- 17 K. Scida, P. W. Stege, G. Haby, G. A. Messina and C. D. García, *Anal. Chim. Acta*, 2011, **691**, 6–17.
- 18 C. N. R. Rao, B. Satishkumar, A. Govindaraj and M. Nath, *ChemPhysChem*, 2001, **2**, 78–105.
- 19 R. H. Baughman, A. A. Zakhidov and W. A. De Heer, *Science*, 2002, **297**, 787–792.
- 20 Z. Liu and X.-J. Liang, *Theranostics*, 2012, **2**, 235.
- 21 L. Dai, D. W. Chang, J. B. Baek and W. Lu, *Small*, 2012, **8**, 1130–1166.
- 22 S. Mouras, A. Hamm, D. Djurado and J.-C. Cousseins, *Rev. Chim. Miner.*, 1987, **24**, 572–582.
- 23 K. Erickson, R. Erni, Z. Lee, N. Alem, W. Gannett and A. Zettl, *Adv. Mater.*, 2010, **22**, 4467–4472.
- 24 K. S. Novoselov, A. K. Geim, S. V. Morozov, D. Jiang, M. I. Katsnelson, I. Grigorieva, S. Dubonos and A. A. Firsov, *Nature*, 2005, **438**, 197–200.
- 25 J. Liu, S. Guo, L. Han, T. Wang, W. Hong, Y. Liu and E. Wang, *J. Mater. Chem.*, 2012, **22**, 20634–20640.
- 26 L. Tang, Y. Wang and J. Li, *Chem. Soc. Rev.*, 2015, **44**, 6954–6980.
- 27 Y. Shao, J. Wang, H. Wu, J. Liu, I. A. Aksay and Y. Lin, *Electroanalysis*, 2010, **22**, 1027–1036.
- 28 T. P. D. Shareena, D. McShan, A. K. Dasmahapatra and P. B. Tchounwou, *Nano-Micro Lett.*, 2018, **10**, 1–34.
- 29 P. R. Wallace, *Phys. Rev.*, 1947, **71**, 622.
- 30 J. Ping, R. Vishnubhotla, A. Vrudhula and A. C. Johnson, *ACS Nano*, 2016, **10**, 8700–8704.
- 31 S. Iijima, *Nature*, 1991, **354**, 56–58.
- 32 S. B. Sinnott and R. Andrews, *Crit. Rev. Solid State Mater. Sci.*, 2001, **26**, 145–249.
- 33 C.-M. Tilmaciu and M. C. Morris, *Front. Chem.*, 2015, **3**, 59.
- 34 P. Ajayan and T. Ebbesen, *Rep. Prog. Phys.*, 1997, **60**, 1025.
- 35 A. Eatemadi, H. Daraee, H. Karimkhanloo, M. Kouhi, N. Zarghami, A. Akbarzadeh, M. Abasi, Y. Hanifehpour and S. W. Joo, *Nanoscale Res. Lett.*, 2014, **9**, 1–13.
- 36 H. Zhu, C. Xu, D. Wu, B. Wei, R. Vajtai and P. Ajayan, *Science*, 2002, **296**, 884–886.
- 37 L. Chico, V. H. Crespi, L. X. Benedict, S. G. Louie and M. L. Cohen, *Phys. Rev. Lett.*, 1996, **76**, 971.
- 38 B.-S. Kong, D.-H. Jung, S.-K. Oh, C.-S. Han and H.-T. Jung, *J. Phys. Chem. C*, 2007, **111**, 8377–8382.
- 39 Q.-M. Feng, J.-B. Pan, H.-R. Zhang, J.-J. Xu and H.-Y. Chen, *Chem. Commun.*, 2014, **50**, 10949–10951.
- 40 B. Shobha and N. Muniraj, *Microsyst. Technol.*, 2015, **21**, 791–800.
- 41 J. Chen, M. A. Hamon, H. Hu, Y. Chen, A. M. Rao, P. C. Eklund and R. C. Haddon, *Science*, 1998, **282**, 95–98.
- 42 V. C. Moore, M. S. Strano, E. H. Haroz, R. H. Hauge, R. E. Smalley, J. Schmidt and Y. Talmon, *Nano Lett.*, 2003, **3**, 1379–1382.



- 43 A. A. Boghossian, J. Zhang, P. W. Barone, N. F. Reuel, J. H. Kim, D. A. Heller, J. H. Ahn, A. J. Hilmer, A. Rwei and J. R. Arkalgud, *ChemSusChem*, 2011, **4**, 848.
- 44 N. M. Iverson, P. W. Barone, M. Shandell, L. J. Trudel, S. Sen, F. Sen, V. Ivanov, E. Atolia, E. Farias and T. P. McNicholas, *Nat. Nanotechnol.*, 2013, **8**, 873–880.
- 45 S. Armenta and F. A. Esteve-Turrillas, *Handbook of Smart Materials in Analytical Chemistry*, 2019, vol. 345, p. 9781119422587.
- 46 M. Dresselhaus and G. Dresslhaus, *Annu. Rev. Mater. Sci.*, 1995, **25**, 487–523.
- 47 H. W. Kroto, J. R. Heath, S. C. O'Brien, R. F. Curl and R. E. Smalley, *Nature*, 1985, **318**, 162–163.
- 48 H. Yi, G. Zeng, C. Lai, D. Huang, L. Tang, J. Gong, M. Chen, P. Xu, H. Wang and M. Cheng, *Chem. Eng. J.*, 2017, **330**, 134–145.
- 49 D. Jariwala, V. K. Sangwan, L. J. Lauhon, T. J. Marks and M. C. Hersam, *Chem. Soc. Rev.*, 2013, **42**, 2824–2860.
- 50 F. L. De La Puente and J.-F. Nierengarten, *Fullerenes: principles and applications*, Royal Society of Chemistry, 2011.
- 51 J. Shinar, *Optical and electronic properties of fullerenes and fullerene-based materials*, CRC Press, 1999.
- 52 G. Churilov, A. Fedorov and P. Novikov, *Carbon*, 2003, **41**, 173–178.
- 53 L. T. Scott, P.-C. Cheng, M. M. Hashemi, M. S. Bratcher, D. T. Meyer and H. B. Warren, *J. Am. Chem. Soc.*, 1997, **119**, 10963–10968.
- 54 J. Gonzalez-Aguilar, M. Moreno and L. Fulcheri, *J. Phys. D: Appl. Phys.*, 2007, **40**, 2361.
- 55 J. R. Baena, M. Gallego and M. Valcarcel, *TrAC, Trends Anal. Chem.*, 2002, **21**, 187–198.
- 56 V. Biju, *Chem. Soc. Rev.*, 2014, **43**, 744–764.
- 57 S. Afreen, K. Muthoosamy, S. Manickam and U. Hashim, *Biosens. Bioelectron.*, 2015, **63**, 354–364.
- 58 V. G. Gavalas and N. A. Chaniotakis, *Anal. Chim. Acta*, 2000, **409**, 131–135.
- 59 K. Saeedfar, L. Y. Heng, T. L. Ling and M. Rezayi, *Sensors*, 2013, **13**, 16851–16866.
- 60 S. Pilehvar and K. De Wael, *Biosensors*, 2015, **5**, 712–735.
- 61 M. Tuerhong, X. Yang and Y. Xue-Bo, *Chin. J. Anal. Chem.*, 2017, **45**, 139–150.
- 62 S. N. Baker and G. A. Baker, *Angew. Chem., Int. Ed.*, 2010, **49**, 6726–6744.
- 63 Y.-P. Sun, B. Zhou, Y. Lin, W. Wang, K. S. Fernando, P. Pathak, M. J. Mezziani, B. A. Harruff, X. Wang and H. Wang, *J. Am. Chem. Soc.*, 2006, **128**, 7756–7757.
- 64 X. Xu, R. Ray, Y. Gu, H. J. Ploehn, L. Gearheart, K. Raker and W. A. Scrivens, *J. Am. Chem. Soc.*, 2004, **126**, 12736–12737.
- 65 J. Shen, Y. Zhu, X. Yang and C. Li, *Chem. Commun.*, 2012, **48**, 3686–3699.
- 66 D. B. Shinde and V. K. Pillai, *Chem. – Eur. J.*, 2012, **18**, 12522–12528.
- 67 H. Li, X. He, Y. Liu, H. Huang, S. Lian, S.-T. Lee and Z. Kang, *Carbon*, 2011, **49**, 605–609.
- 68 F. Wang, S. Pang, L. Wang, Q. Li, M. Kreiter and C.-Y. Liu, *Chem. Mater.*, 2010, **22**, 4528–4530.
- 69 J. Deng, Q. Lu, N. Mi, H. Li, M. Liu, M. Xu, L. Tan, Q. Xie, Y. Zhang and S. Yao, *Chem. – Eur. J.*, 2014, **20**, 4993–4999.
- 70 A. Cayuela, M. Soriano, C. Carrillo-Carrión and M. Valcárcel, *Chem. Commun.*, 2016, **52**, 1311–1326.
- 71 S. Ray, A. Saha, N. R. Jana and R. Sarkar, *J. Phys. Chem. C*, 2009, **113**, 18546–18551.
- 72 R. Shen, K. Song, H. Liu, Y. Li and H. Liu, *ChemPhysChem*, 2012, **13**, 3549–3555.
- 73 S.-T. Yang, X. Wang, H. Wang, F. Lu, P. G. Luo, L. Cao, M. J. Mezziani, J.-H. Liu, Y. Liu and M. Chen, *J. Phys. Chem. C*, 2009, **113**, 18110–18114.
- 74 X. Zhai, P. Zhang, C. Liu, T. Bai, W. Li, L. Dai and W. Liu, *Chem. Commun.*, 2012, **48**, 7955–7957.
- 75 S. Liu, B. Yu and T. Zhang, *RSC Adv.*, 2014, **4**, 544–548.
- 76 M. Vedamalai, A. P. Periasamy, C.-W. Wang, Y.-T. Tseng, L.-C. Ho, C.-C. Shih and H.-T. Chang, *Nanoscale*, 2014, **6**, 13119–13125.
- 77 P. Miao, L. Liu, Y. Li and G. Li, *Electrochem. Commun.*, 2009, **11**, 1904–1907.
- 78 X. Qin, W. Lu, A. M. Asiri, A. O. Al-Youbi and X. Sun, *Sens. Actuators, B*, 2013, **184**, 156–162.
- 79 J. Zhao, Y. Yan, L. Zhu, X. Li and G. Li, *Biosens. Bioelectron.*, 2013, **41**, 815–819.
- 80 S. Iijima, M. Yudasaka, R. Yamada, S. Bandow, K. Suenaga, F. Kokai and K. Takahashi, *Chem. Phys. Lett.*, 1999, **309**, 165–170.
- 81 B.-C. Serban, M. Bumbac, O. Buiu, C. Cobianu, M. Brezeanu and C. Nicolescu, *Ann. Acad. Rom. Sci. Ser. Math. Appl.*, 2018, **11**, 5–18.
- 82 S. Zhu and G. Xu, *Nanoscale*, 2010, **2**, 2538–2549.
- 83 N. Karousis, I. Suarez-Martinez, C. P. Ewels and N. Tagmatarchis, *Chem. Rev.*, 2016, **116**, 4850–4883.
- 84 X. Liu, L. Shi, W. Niu, H. Li and G. Xu, *Biosens. Bioelectron.*, 2008, **23**, 1887–1890.
- 85 X. Liu, H. Li, F. Wang, S. Zhu, Y. Wang and G. Xu, *Biosens. Bioelectron.*, 2010, **25**, 2194–2199.
- 86 A. Datta, M. Kirca, Y. Fu and A. C. To, *Nanotechnology*, 2011, **22**, 065706.
- 87 V. Georgakilas, J. A. Perman, J. Tucek and R. Zboril, *Chem. Rev.*, 2015, **115**, 4744–4822.
- 88 K. Volkov, V. Danilenko and V. Elin, *Fiz. Goreniya Vzryva*, 1990, **26**, 123–125.
- 89 R. P. Mildren, *Opt. Eng. Diamond*, 2013, **1**, 1–34.
- 90 G. Painter, D. E. Ellis and A. Lubinsky, *Phys. Rev. B: Solid State*, 1971, **4**, 3610.
- 91 Y. Zhang, K. Y. Rhee, D. Hui and S.-J. Park, *Composites, Part B*, 2018, **143**, 19–27.
- 92 Y. Wang, M. Jaiswal, M. Lin, S. Saha, B. Ozyilmaz and K. P. Loh, *ACS Nano*, 2012, **6**, 1018–1025.
- 93 M. H. Abouzar, A. Poghossian, A. Razavi, O. A. Williams, N. Bijnens, P. Wagner and M. J. Schöning, *Biosens. Bioelectron.*, 2009, **24**, 1298–1304.
- 94 J. Narayan and A. Bhaumik, *Mater. Res. Lett.*, 2017, **5**, 242–250.



- 95 P. Joshi, R. Mishra and R. J. Narayan, *Curr. Opin. Biomed. Eng.*, 2021, **18**, 100274.
- 96 M. J. Wang, C. A. Gray, S. A. Reznick, K. Mahmud and Y. Kutsovsky, *Kirk-Othmer Encyclopedia of Chemical Technology*, 2000.
- 97 F. Arduini, M. Forchielli, A. Amine, D. Neagu, I. Cacciotti, F. Nanni, D. Moscone and G. Palleschi, *Microchim. Acta*, 2015, **182**, 643–651.
- 98 R. Eivazzadeh-Keihan, E. B. Noruzi, E. Chidar, M. Jafari, F. Davoodi, A. Kashtiaray, M. G. Gorab, S. M. Hashemi, S. Javanshir and R. A. Cohan, *Chem. Eng. J.*, 2022, 136183.
- 99 M. Inagaki, Y. Yang and F. Kang, *Adv. Mater.*, 2012, **24**, 2547–2566.
- 100 K. P. De Jong and J. W. Geus, *Catal. Rev.: Sci. Eng.*, 2000, **42**, 481–510.
- 101 L. Feng, N. Xie and J. Zhong, *Materials*, 2014, **7**, 3919–3945.
- 102 V. Vamvakaki, K. Tsagaraki and N. Chaniotakis, *Anal. Chem.*, 2006, **78**, 5538–5542.
- 103 L. Wu, M. McIntosh, X. Zhang and H. Ju, *Talanta*, 2007, **74**, 387–392.
- 104 L. Wu, X. Zhang and H. Ju, *Biosens. Bioelectron.*, 2007, **23**, 479–484.
- 105 A. Arvinte, F. Valentini, A. Radoi, F. Arduini, E. Tamburri, L. Rotariu, G. Palleschi and C. Bala, *Electroanalysis*, 2007, **19**, 1455–1459.
- 106 Y. Mei, C. He, W. Zeng, Y. Luo, C. Liu, M. Yang, Y. Kuang, X. Lin and Q. Huang, *Food Bioprocess Technol.*, 2022, 1–16.
- 107 J. N. Tiwari, V. Vij, K. C. Kemp and K. S. Kim, *ACS Nano*, 2016, **10**, 46–80.
- 108 A. Ambrosi, C. K. Chua, A. Bonanni and M. Pumera, *Chem. Rev.*, 2014, **114**, 7150–7188.
- 109 V. N. Ataide, I. V. Arantes, L. F. Mendes, D. S. Rocha, T. A. Baldo, W. K. Coltro and T. R. Paixão, *J. Electrochem. Soc.*, 2022, **169**, 047524.
- 110 T. Pasinszki, M. Krebsz, T. T. Tung and D. Losic, *Sensors*, 2017, **17**, 1919.
- 111 L. Wang, Q. Xiong, F. Xiao and H. Duan, *Biosens. Bioelectron.*, 2017, **89**, 136–151.
- 112 M. Hasanzadeh and N. Shadjou, *Mater. Sci. Eng., C*, 2017, **71**, 1313–1326.
- 113 T. T. Tung, M. J. Nine, M. Krebsz, T. Pasinszki, C. J. Coghlan, D. N. Tran and D. Losic, *Adv. Funct. Mater.*, 2017, **27**, 1702891.
- 114 B. V. Chikkaveeraiah, A. A. Bhirde, N. Y. Morgan, H. S. Eden and X. Chen, *ACS Nano*, 2012, **6**, 6546–6561.
- 115 Y. Wu, P. Xue, Y. Kang and K. M. Hui, *Anal. Chem.*, 2013, **85**, 8661–8668.
- 116 U. Anand, A. K. S. Chandel, P. Oleksak, A. Mishra, O. Krejcar, I. H. Raval, A. Dey and K. Kuca, *Appl. Microbiol. Biotechnol.*, 2022, 1–27.
- 117 B. Esteban-Fernandez de Avila, E. Araque, S. Campuzano, M. Pedrero, B. Dalkiran, R. Barderas, R. Villalonga, E. Kilic and J. M. Pingarron, *Anal. Chem.*, 2015, **87**, 2290–2298.
- 118 T. Kilic, A. Erdem, Y. Erac, M. O. Seydibeyoglu, S. Okur and M. Ozsoz, *Electroanalysis*, 2015, **27**, 317–326.
- 119 T. Wei, W. Tu, B. Zhao, Y. Lan, J. Bao and Z. Dai, *Sci. Rep.*, 2014, **4**, 1–7.
- 120 H. W. Yang, C. W. Lin, M. Y. Hua, S. S. Liao, Y. T. Chen, H. C. Chen, W. H. Weng, C. K. Chuang, S. T. Pang and C. C. M. Ma, *Adv. Mater.*, 2014, **26**, 3662–3666.
- 121 S. Kumar, J. G. Sharma, S. Maji and B. D. Malhotra, *Biosens. Bioelectron.*, 2016, **78**, 497–504.
- 122 R. Heidari, J. Rashidiani, M. Abkar, R. A. Taheri, M. M. Moghaddam, S. A. Mirhosseini, R. Seidmoradi, M. R. Nourani, M. Mahboobi and A. H. Keihan, *Biosens. Bioelectron.*, 2019, **126**, 7–14.
- 123 M. Chen, Y. Wang, H. Su, L. Mao, X. Jiang, T. Zhang and X. Dai, *Sens. Actuators, B*, 2018, **255**, 2910–2918.
- 124 Y. Wang, X. Li, W. Cao, Y. Li, H. Li, B. Du and Q. Wei, *Biosens. Bioelectron.*, 2014, **61**, 618–624.
- 125 S. Hammarström, E. Engvall, B. G. Johansson, S. Svensson, G. Sundblad and I. J. Goldstein, *Proc. Natl. Acad. Sci. U. S. A.*, 1975, **72**, 1528–1532.
- 126 A. M. Ballesta, R. Molina, X. Filella, J. Jo and N. Giménez, *Tumor Biol.*, 1995, **16**, 32–41.
- 127 F. Naghibalhossaini and P. Ebadi, *Cancer Lett.*, 2006, **234**, 158–167.
- 128 F. Li, L. Jiang, J. Han, Q. Liu, Y. Dong, Y. Li and Q. Wei, *RSC Adv.*, 2015, **5**, 19961–19969.
- 129 X. Pang, J. Li, Y. Zhao, D. Wu, Y. Zhang, B. Du, H. Ma and Q. Wei, *ACS Appl. Mater. Interfaces*, 2015, **7**, 19260–19267.
- 130 J. Han, Y. Li, J. Feng, M. Li, P. Wang, Z. Chen and Y. Dong, *J. Electroanal. Chem.*, 2017, **786**, 112–119.
- 131 E. Heydari-Bafrooei and N. S. Shamszadeh, *Biosens. Bioelectron.*, 2017, **91**, 284–292.
- 132 Y. Wang, Y. Qu, X. Ye, K. Wu and C. Li, *J. Solid State Electrochem.*, 2016, **20**, 2217–2222.
- 133 F. Li, J. Peng, J. Wang, H. Tang, L. Tan, Q. Xie and S. Yao, *Biosens. Bioelectron.*, 2014, **54**, 158–164.
- 134 A. Sabahi, R. Salahandish, A. Ghaffarinejad and E. Omidinia, *Talanta*, 2020, **209**, 120595.
- 135 Y. Luo, Y. Wang, H. Yan, Y. Wu, C. Zhu, D. Du and Y. Lin, *Anal. Chim. Acta*, 2018, **1042**, 44–51.
- 136 P. Gulati, P. Mishra, M. Khanuja, J. Narang and S. Islam, *Process Biochem.*, 2020, **90**, 184–192.
- 137 M. Chen, D. Wu, S. Tu, C. Yang, D. Chen and Y. Xu, *Sci. Rep.*, 2021, **11**, 1–11.
- 138 D. Wu, Y. Liu, Y. Wang, L. Hu, H. Ma, G. Wang and Q. Wei, *Sci. Rep.*, 2016, **6**, 1–7.
- 139 L. Li, W. Li, C. Ma, H. Yang, S. Ge and J. Yu, *Sens. Actuators, B*, 2014, **202**, 314–322.
- 140 H. Yang, W. Liu, C. Ma, Y. Zhang, X. Wang, J. Yu and X. Song, *Electrochim. Acta*, 2014, **123**, 470–476.
- 141 T. Hu, L. Zhang, W. Wen, X. Zhang and S. Wang, *Biosens. Bioelectron.*, 2016, **77**, 451–456.
- 142 V. Serafín, A. Valverde, G. Martínez-García, E. Martínez-Periñán, F. Comba, M. Garranzo-Asensio, R. Barderas, P. Yáñez-Sedeño, S. Campuzano and J. Pingarrón, *Sens. Actuators, B*, 2019, **284**, 711–722.
- 143 L. Wang, Y. Zhang, A. Wu and G. Wei, *Anal. Chim. Acta*, 2017, **985**, 24–40.



- 144 X. Guo, *J. Biophotonics*, 2012, **5**, 483–501.
- 145 Q. Wang, Q. Li, X. Yang, K. Wang, S. Du, H. Zhang and Y. Nie, *Biosens. Bioelectron.*, 2016, **77**, 1001–1007.
- 146 M. Hossain, M. Islam, L. F. Abdulrazak, M. Rana, T. B. A. Akib and M. Hassan, *Photonic Sens.*, 2020, **10**, 67–79.
- 147 N.-F. Chiu, T.-L. Lin and C.-T. Kuo, *Sens. Actuators, B*, 2018, **265**, 264–272.
- 148 L. He, Q. Pagneux, I. Larroulet, A. Y. Serrano, A. Pesquera, A. Zurutuza, D. Mandler, R. Boukherroub and S. Szunerits, *Biosens. Bioelectron.*, 2017, **89**, 606–611.
- 149 F. Xing, G.-X. Meng, Q. Zhang, L.-T. Pan, P. Wang, Z.-B. Liu, W.-S. Jiang, Y. Chen and J.-G. Tian, *Nano Lett.*, 2014, **14**, 3563–3569.
- 150 B. Muthuraj, S. Mukherjee, S. R. Chowdhury, C. R. Patra and P. K. Iyer, *Biosens. Bioelectron.*, 2017, **89**, 636–644.
- 151 R. M. Williams, C. Lee and D. A. Heller, *ACS Sens.*, 2018, **3**, 1838–1845.
- 152 V. Gedi, C. K. Song, G. B. Kim, J. O. Lee, E. Oh, B. S. Shin, M. Jung, J. Shim, H. Lee and Y.-P. Kim, *Sens. Actuators, B*, 2018, **256**, 89–97.
- 153 J. D. Harvey, P. V. Jena, H. A. Baker, G. H. Zerbe, R. M. Williams, T. V. Galassi, D. Roxbury, J. Mittal and D. A. Heller, *Nat. Biomed. Eng.*, 2017, **1**, 1–11.
- 154 P. Gulati, P. Kaur, M. Rajam, T. Srivastava, M. A. Ali, P. Mishra and S. Islam, *Sens. Actuators, B*, 2018, **270**, 45–55.
- 155 M. J. Burger, M. A. Tebay, P. A. Keith, H. M. Samarutunga, J. Clements, M. F. Lavin and R. A. Gardiner, *Int. J. Cancer*, 2002, **100**, 228–237.
- 156 A. Juzgado, A. Soldà, A. Ostric, A. Criado, G. Valenti, S. Rapino, G. Conti, G. Fracasso, F. Paolucci and M. Prato, *J. Mater. Chem. B*, 2017, **5**, 6681–6687.
- 157 Y. Xia, M. Liu, L. Wang, A. Yan, W. He, M. Chen, J. Lan, J. Xu, L. Guan and J. Chen, *Biosens. Bioelectron.*, 2017, **92**, 8–15.
- 158 Y. Huang, M. Shi, K. Hu, S. Zhao, X. Lu, Z.-F. Chen, J. Chen and H. Liang, *J. Mater. Chem. B*, 2013, **1**, 3470–3476.
- 159 O. S. Wolfbeis, *Chem. Soc. Rev.*, 2015, **44**, 4743–4768.
- 160 F. Khakbaz and M. Mahani, *Anal. Biochem.*, 2017, **523**, 32–38.
- 161 S. Lu, G. Li, Z. Lv, N. Qiu, W. Kong, P. Gong, G. Chen, L. Xia, X. Guo and J. You, *Biosens. Bioelectron.*, 2016, **85**, 358–362.
- 162 D. Qin, X. Jiang, G. Mo, J. Feng, C. Yu and B. Deng, *ACS Sens.*, 2019, **4**, 504–512.
- 163 M. Zhang, H. Liu, L. Chen, M. Yan, L. Ge, S. Ge and J. Yu, *Biosens. Bioelectron.*, 2013, **49**, 79–85.
- 164 S. Mohammadi and A. Salimi, *Microchim. Acta*, 2018, **185**, 1–10.
- 165 Y. Ding, J. Ling, H. Wang, J. Zou, K. Wang, X. Xiao and M. Yang, *Anal. Methods*, 2015, **7**, 7792–7798.
- 166 K. Mintz, E. Waidely, Y. Zhou, Z. Peng, A. O. Al-Youbi, A. S. Bashammakh, M. S. El-Shahawi and R. M. Leblanc, *Anal. Chim. Acta*, 2018, **1041**, 114–121.

